bioRxiv preprint doi: https://doi.org/10.1101/2023.04.04.535582; this version posted April 4, 2023. The copyright holder for this preprint (which was not certified by peer review) is the author/funder, who has granted bioRxiv a license to display the preprint in perpetuity. It is made available under aCC-BY-NC-ND 4.0 International license.

Activation of a *Vibrio cholerae* CBASS anti-phage system by quorum sensing and folate depletion

Geoffrey B. Severin[1#], Miriam S. Ramliden[2], Kathryne C. Ford[3], Andrew J. Van Alst[3], Ram Sanath-Kumar[3], Kaitlin A. Decker[3], Brian Y. Hsueh[3], Soo Hun Yoon[3], Lucas M. Demey[3], Brendan J. O'Hara [2], Christopher R. Rhoades[3], Victor J. DiRita[3], Wai-Leung Ng[2], and Christopher M. Waters[3*]

[1]Department of Biochemistry and Molecular Biology, Michigan State University, East Lansing, Michigan, USA, 48824

[2]Department of Molecular Biology and Microbiology, Tufts University School of Medicine, Boston, Massachusetts, USA

[3]Department of Microbiology and Molecular Genetics, Michigan State University, East Lansing, Michigan, USA

[#]Current Address, Department of Microbiology and Immunology, University of Michigan, Ann Arbor, Michigan, USA

[*]**Corresponding Author:**

5180 Biomedical and Physical Sciences

567 Wilson Road

East Lansing, MI 48824

Telephone 517-884-5360

bioRxiv preprint doi: https://doi.org/10.1101/2023.04.04.535582; this version posted April 4, 2023. The copyright holder for this preprint (which was not certified by peer review) is the author/funder, who has granted bioRxiv a license to display the preprint in perpetuity. It is made available under aCC-BY-NC-ND 4.0 International license.

E-mail: watersc3@msu.edu

Short title: Folate and QS regulation of CBASS

Key Words: cyclic GMP-AMP; CD-NTases; phage; quorum sensing; folate

Declarations of interest: none

Abstract

A major challenge faced by bacteria is infection by bacteriophage (phage). Abortive infection is one strategy for combating phage in which an infected cell kills itself to limit phage replication, thus protecting neighboring kin. One class of abortive infection systems is the cyclic oligonucleotide based anti-phage signaling system (CBASS) which relies on two core enzymatic activities; an oligo-nucleotide cyclase that is activated following phage infection and a cyclic-oligo-nucleotide sensitive effector whose activity kills the infected cell. However, the mechanisms behind the deployment and activation of these lethal CBASS systems prior-to and following infection have largely remained a mystery. While exploring unique genomic features of the current pandemic *Vibrio cholerae* biotype El Tor for clues underlying its pandemic success we found its CBASS was spuriously activated by the folate biosynthesis inhibitor sulfamethoxazole, but only after the population had reached a high-cell density. This population density dependent activity revealed that transcription of both the oligo-nucleotide cyclase, *dncV*, and the CBASS phospholipase effector, *capV*, is enhanced at high-cell density by quorum sensing. Together, these results demonstrate that the *V. cholerae* CBASS is deployed when the

bioRxiv preprint doi: https://doi.org/10.1101/2023.04.04.535582; this version posted April 4, 2023. The copyright holder for this preprint (which was not certified by peer review) is the author/funder, who has granted bioRxiv a license to display the preprint in perpetuity. It is made available under aCC-BY-NC-ND 4.0 International license.

environment is densely populated and activated in response to a perturbation in folate biosynthesis.

Significance

To counteract infection with phage, bacteria have evolved a myriad of molecular defense systems. Some of these systems initiate a process called abortive infection, in which the infected cell kills itself to prevent phage propagation. However, such systems must be inhibited in the absence of phage infection to prevent spurious death of the host. Here we show that the cyclic oligonucleotide based anti-phage signaling system (CBASS) accomplishes this by sensing intracellular folate molecules and only expressing this system in a group. These results enhance our understanding of the evolution of the 7th *V. cholerae* pandemic and more broadly how bacteria defend themselves against phage infection.

Introduction

The diarrheal disease cholera, caused by the Gram-negative bacterium *Vibrio cholerae*, is spread through consumption of contaminated food and water (1). Of the seven recorded cholera pandemics the classical biotype is believed to have caused at a minimum both the 5th (1881 - 1896) and 6th (1899 - 1923) pandemics whereas the El Tor biotype is responsible for initiating and perpetuating the 7th pandemic (1961 - today) (2, 3). While strains of the classical biotype are now rarely encountered in environmental and clinical settings, numerous assays have been developed to help distinguish *V. cholerae* isolates as belonging to either the classical or El Tor biotypes (4, 5). These include disparate growth on citrate, hemolytic activity, casein proteolysis,

bioRxiv preprint doi: https://doi.org/10.1101/2023.04.04.535582; this version posted April 4, 2023. The copyright holder for this preprint (which was not certified by peer review) is the author/funder, who has granted bioRxiv a license to display the preprint in perpetuity. It is made available under aCC-BY-NC-ND 4.0 International license.

production of acidic or neutral byproducts from growth on glucose, differences in virulence gene allele sequences and expression, and disparate sensitivities to the cationic antimicrobial peptide polymyxin B and the folate biosynthesis inhibitor sulfamethoxazole (SMX).

Two of the largest genetic differences between the *V. cholerae* biotypes are the Vibrio Seventh Pandemic Islands 1 and 2 (VSP-1 and 2) genomic islands that are defining features of the El Tor biotype and absent in the classical biotype (3, 6, 7). VSP-1 and 2, which collectively contain ~36 genes, are hypothesized to have played a critical role in the pandemic evolution of the El Tor biotype and many recent studies have begun to explore the biological functions they encode. The predominant function of these islands appears to be protection against invasive biological elements as two phage defense systems, AvcID (8, 9) and a Type II cyclic oligonucleotide based anti-phage signaling system (CBASS) (10–13), are encoded on VSP-1 while VSP-2 encodes the *ddmABC* operon, which inhibits plasmid acquisition, plasmid stability, and phage invasion (14, 15). In addition to biological defense, a three gene operon on VSP-2 that is encoded in some strains of El Tor mediates aerotaxis in response to zinc (16). Outside of these four systems, little is known of the function of the VSP islands or their contribution to the emergence of the El Tor biotype.

The VSP-1 CBASS encompasses a four gene operon [*vc0178(capV)-vc0179(dncV)-vc0180(cap2)-vc0181(cap3)*]. In this system, via an unknown mechanism, phage infection stimulates DncV, a member of the CD-NTase family of enzymes (17), to synthesize of 3’3’ cyclic GMP-AMP (cGAMP) (11, 18). cGAMP then allosterically activates the phospholipase CapV, which rapidly degrades

bioRxiv preprint doi: https://doi.org/10.1101/2023.04.04.535582; this version posted April 4, 2023. The copyright holder for this preprint (which was not certified by peer review) is the author/funder, who has granted bioRxiv a license to display the preprint in perpetuity. It is made available under aCC-BY-NC-ND 4.0 International license.

the infected cell's own membrane (10). Cap2 enhances the production of cGAMP by post translationally modifying the C-terminus of DncV in a manner analogous to ubiquitination (12, 13). Conversely, Cap3 suppresses DncV activity by precisely proteolyzing this same C-terminal modification (12, 13). Ultimately, activation of VSP-1 CBASS rapidly kills the infected cell to restrict phage propagation and protect neighboring kin from further phage predation, a mechanism called abortive infection (11). While CBASS systems are widely encoded in bacterial genomes (11, 17, 19), we are just beginning to learn how these lethal population-level phage defense systems are controlled.

Bacteria sense their population density through quorum sensing (QS). Based on the constituency and abundance of bacteria in the environment, a bacterium uses QS to enact gene expression patterns that promote or discourage participation in coordinated population-level behaviors (reviewed in (20, 21)). Bacteria assess the local population density and composition by producing, secreting, and detecting small molecules called auto-inducers (AIs) whose environmental concentrations are a proxy for bacterial abundance. In *V. cholerae*, QS gene expression programs for low-cell density (LCD) and high-cell density (HCD) are regulated by the transcription factors LuxO and HapR, respectively. At LCD, when the environmental concentrations of AIs are low, LuxO is active and *hapR* mRNA is degraded. As AI concentrations increase in the environment, a proxy for an increasing population density, LuxO activity is inhibited via dephosphorylation, driving *hapR* expression and enabling induction of the HCD gene expression regulon. The dichotomous QS-dependent activities of LuxO and HapR are primarily responsible for the differential regulation of more than 500 *V. cholerae* genes (22).

bioRxiv preprint doi: https://doi.org/10.1101/2023.04.04.535582; this version posted April 4, 2023. The copyright holder for this preprint (which was not certified by peer review) is the author/funder, who has granted bioRxiv a license to display the preprint in perpetuity. It is made available under aCC-BY-NC-ND 4.0 International license.

These population-dependent changes in transcription determine whether *V. cholerae* pursue behavioral strategies best suited for a solitary or group lifestyle at LCD or HCD.

To better understand the contribution of the VSP islands to the evolution of the 7th *V. cholerae* pandemic, we explored if the VSP islands in the El Tor biotype were responsible for some of the well-known phenotypic differences between strains of the classical and El Tor biotypes. We report that El Tor's sensitivity to the folate biosynthesis inhibitor SMX is dependent on the VSP-1 encoded Type-II CBASS. This sensitivity results from the spurious activation of DncV and the subsequent activation of the phospholipase CapV. Furthermore, during these studies we found that the expression of *dncV* and *capV* are induced at HCD by the *V. cholerae* QS pathway, consistent with its function as a population-level phage defense mechanism. Our findings identify both transcriptional and post-transcriptional mechanisms that lead to the deployment and activation of the El Tor *V. cholerae* CBASS.

Results

VSP-1 and -2 do not impact metabolic phenotypes commonly used to distinguish the El Tor and classical *V. cholerae* biotypes

We examined whether the VSP-1 and VSP-2 islands contributed to phenotypic behaviors commonly attributed to the El Tor biotype by performing several biotyping assays comparing classical strain O395 (23) and the El Tor strain C6706str2 (C6706) (24) with those of single VSP island mutants (ΔVSP-1 and ΔVSP-2) and a double VSP island mutant (ΔVSP1/2). O395 is known to be deficient in both protease and hemolysin production in comparison to C6706, as

bioRxiv preprint doi: https://doi.org/10.1101/2023.04.04.535582; this version posted April 4, 2023. The copyright holder for this preprint (which was not certified by peer review) is the author/funder, who has granted bioRxiv a license to display the preprint in perpetuity. It is made available under aCC-BY-NC-ND 4.0 International license.

demonstrated on casein milk agar and blood agar plates, respectively (4). Simple streaks of these strains on milk agar and sheep blood agar confirmed differential degradation of casein and hemolytic activities between O395 and C6706, as indicated by the absence and presence of a zone of clearing on each medium, respectively (Figs. 1A & 1B). We found that deletion of one or both VSP islands did not affect either activity as all three mutants phenocopied the parental C6706 strain (Figs. 1A & 1B). Similarly, classical O395 cannot utilize citrate as a sole carbon source (25) or grow on MacConkey agar, while C6706 can do both. Again, we found that the VSP islands do not contribute to these two phenotypes as all three mutants grew comparably to the parental C6706 strain on these media (Figs. 1C and 1D). Finally, El Tor strains are known to produce acetoin upon fermentation of glucose while classical strains do not (26). Using the colorimetric Voges-Proskauer assay to measure acetoin by the generation of a red color, we found supernatants of C6706 produced a deep red color, indicative of acetoin production, while classical O395 was weakly pink (Fig. 1E). Production of acetoin was not grossly impacted upon deletion of either or both VSP islands (Fig. 1E) as these strains also produced a deep red color like the parental C6706. While casein degradation in milk agar and production of the fermentative bioproduct acetoin have been linked to QS (4, 27) and the inability of O395 to perform these functions is likely due, in-part, to its non-functional *hapR* allele (28), we nonetheless demonstrate the VSP islands do not contribute to these phenotypes in C6706.

The VSP-1 and -2 islands do not contribute to El Tor C6706 colonization in an infant mouse model

bioRxiv preprint doi: https://doi.org/10.1101/2023.04.04.535582; this version posted April 4, 2023. The copyright holder for this preprint (which was not certified by peer review) is the author/funder, who has granted bioRxiv a license to display the preprint in perpetuity. It is made available under aCC-BY-NC-ND 4.0 International license.

Subtle differences in the sequences of the virulence gene alleles *ctxB* and *tcpA* between strains of the El Tor and classical biotypes have been used for biotyping novel *V. cholerae* isolates (4). The classical biotype is also more permissive in its in vitro expression of the *V. cholerae* virulence regulon compared to the El Tor biotype (29), which anecdotally causes less severe cholera in humans (30). To determine whether the VSP islands collectively contribute to in vivo colonization we performed a competition infection between C6706 and ΔVSP-1/2 in the infant mouse model of cholera. Despite the previous attribution of *dncV*, the CBASS cGAMP synthase located in VSP-1, to colonization (18), we found no competitive defect in the ability of the double VSP island mutant to colonize the infant mouse intestinal tract (Fig. 1F). The discrepancy between this finding and *Davies et al.* 2012 may be attributed to unknown epistatic relationships between *dncV* and other VSP encoded genes which obscure this colonization defect in our study, genetic differences between laboratory lineages of C6706 (31), or specific conditions not replicated in our study. Nevertheless, our result suggests that the collective impact of the VSP islands on colonization in the infant mouse model of cholera is negligible.

VSP-1 increases sensitivity to sulfamethoxazole

In addition to different metabolic and virulence characteristics, different susceptibilities to antibiotics have also been observed between classical and El Tor strains. One such antibiotic is the cationic antimicrobial peptide polymyxin B, which disrupts the outer membrane of Gram-negative bacteria. Indeed, as previously observed in pandemic *V. cholerae* biotypes (32, 33), we found that classical O395 was more sensitive to polymyxin B than El Tor C6706 with half maximal inhibitory concentrations (IC_{50}) of 0.6 and 18.4 μg/mL, respectively (Fig. S1 , Table S1).

bioRxiv preprint doi: https://doi.org/10.1101/2023.04.04.535582; this version posted April 4, 2023. The copyright holder for this preprint (which was not certified by peer review) is the author/funder, who has granted bioRxiv a license to display the preprint in perpetuity. It is made available under aCC-BY-NC-ND 4.0 International license.

174 However, deletion of VSP-1, VSP-2, or both islands did not grossly impact El Tor's susceptibility
175 to polymyxin B (Fig. S1, Table S1) demonstrating the VSP islands do not contribute to this
176 biotype specific phenotype.
177
178 In contrast to polymyxin B, strains of the El Tor biotype have been shown to exhibit greater
179 sensitivity to sulfamethoxazole (SMX) than those of the classical biotype (5). SMX impairs folate
180 biosynthesis by inhibiting the activity of dihydropteroate synthase. After treating our strains
181 with a concentration gradient of SMX and measuring culture optical densities after 24 hours we
182 found C6706 was profoundly more sensitive to SMX (IC_{50} 36.5 µg/mL) than classical O395 (IC_{50}
183 230.7 µg/mL) (Figs. 2A & S2A, Table S1). Surprisingly, both ΔVSP-1 and ΔVSP-1/2 phenocopied
184 O395's SMX resistance while the ΔVSP-2 mutant retained the parental C6706 SMX sensitivity
185 (Figs. 2A & S2A, Table S1). Hypothesizing SMX sensitivity could be attributed to VSP-1, we
186 reintroduced VSP-1 into the ΔVSP-1/2 mutant on a single copy cosmid (pVSP-1) and found this
187 was sufficient to restore SMX sensitivity (Figs. 2B & S2B). Additionally, provision of pVSP-1 to
188 both O395 and *Escherichia coli* BL21(DE3) also increased each strain's sensitivity to SMX (Figs.
189 2B, S2C & S2D). Together, these results demonstrate the disparity in *V. cholerae* biotype specific
190 sensitivities to SMX is the result of a factor encoded on VSP-1.
191
192 **Sulfamethoxazole sensitivity requires the CBASS genes *dncV* and *capV***
193 The VSP-1 island of *V. cholerae* C6706 contains 12 known or predicted genes (Fig. 2C). To
194 identify which genes are responsible for SMX sensitivity, we challenged three partial VSP-1
195 island mutants (Δ*avcD-vc0176*, Δ*vspR-cap3*, and Δ*vc0182-vc0185*) with a gradient of SMX

bioRxiv preprint doi: https://doi.org/10.1101/2023.04.04.535582; this version posted April 4, 2023. The copyright holder for this preprint (which was not certified by peer review) is the author/funder, who has granted bioRxiv a license to display the preprint in perpetuity. It is made available under aCC-BY-NC-ND 4.0 International license.

196 concentrations and found only the Δ*vspR-cap3* mutant was more resistant to SMX (Figs. 2D &
197 S2E). The five genes missing in this mutant include the negative transcriptional regulator of
198 CBASS, *vspR* (18), and the four gene CBASS (*dncV-cap3*) (11) (Fig. 2C). It was previously shown
199 that folates are allosteric regulators of DncV which suppress cGAMP synthesis in vitro (34) and
200 that cGAMP is required for the activation of the lethal phospholipase CapV (10). We therefore
201 hypothesized that inhibition of folate biosynthesis by SMX could alleviate the folate-dependent
202 repression of DncV activity and lead to CapV-dependent cell death. In support of this
203 hypothesis, deletion of either *dncV* or *capV* was sufficient to enhance resistance to SMX in these
204 conditions while loss of *vspR*, *cap2*, or *cap3* was not (Figs. 2D & S2F).
205
206 **Sulfamethoxazole activates DncV cGAMP synthesis**
207 It was previously reported that the addition of sulfonamide to *E. coli* strains ectopically
208 expressing *dncV* from a high-copy plasmid enhanced the catalytic activity of DncV (34). To test
209 whether SMX treatment might induce cGAMP synthesis by DncV in its native cellular and
210 genetic contexts, we back-diluted stationary phase cultures of C6706 and Δ*capV* 1:1,000 in
211 fresh medium, allowed them to recover for approximately one hour, introduced 100 µg/mL SMX
212 or a DMSO control, and measured culture optical density over the course of six hours.
213 Concurrent with monitoring culture density, we also measured the intracellular concentration of
214 cGAMP using UPLC-MS/MS, but this measurement was only performed in the Δ*capV* cultures
215 where detectable levels of cGAMP can accumulate without inducing CapV-dependent cell lysis
216 (10). Surprisingly, C6706 cultures treated with SMX only exhibited a growth defect after two
217 hours of exposure to the antibiotic (Fig. 3A). This growth defect is a consequence of CapV

bioRxiv preprint doi: https://doi.org/10.1101/2023.04.04.535582; this version posted April 4, 2023. The copyright holder for this preprint (which was not certified by peer review) is the author/funder, who has granted bioRxiv a license to display the preprint in perpetuity. It is made available under aCC-BY-NC-ND 4.0 International license.

activity as there was no difference in growth between Δ*capV* cultures treated with and without SMX (Fig. 3A). Similarly, cGAMP was only found in Δ*capV* cultures challenged with SMX and was not detected until more than two hours after its addition (Fig. 3A). While these results demonstrate that SMX stimulates DncV synthesis of cGAMP in its native environment, they also reveal a profound delay exists between introduction of the antibiotic and evidence of DncV activity under these experimental conditions.

QS contributes to CBASS-dependent SMX sensitivity

Hypothesizing the two-hour delay in SMX-dependent growth inhibition and cGAMP synthesis (Fig. 3A) was an indication of CBASS regulation by QS, we challenged QS mutants locked in LCD or HCD gene expression with 100 μg/mL SMX or a DMSO control and monitored culture densities over time. Because LCD QS mutants have a propensity to form biofilms, which could interfere with measuring optical density, we utilized QS mutants derived from the biofilm-null C6706 Δ*vpsL* background (35). Importantly, there is no difference between C6706 and Δ*vpsL* when challenged with SMX or DMSO in these conditions (Fig. S3). As previously seen for C6706 (Fig. 3A), the Δ*vpsL* cultures with an intact QS system experienced a similar two-hour delay in growth inhibition in response to SMX (Fig. 3B). In agreement with our hypothesis that QS induces CBASS, the LCD-locked Δ*vpsL*Δ*hapR* strain was tolerant of SMX (Figs. 3C) while the HCD-locked Δ*vpsL*Δ*luxO* was hypersensitive to SMX with an abbreviated temporal delay in growth inhibition (Fig. 3D). Together, these results support the argument that QS contributes to the regulation of CBASS.

bioRxiv preprint doi: https://doi.org/10.1101/2023.04.04.535582; this version posted April 4, 2023. The copyright holder for this preprint (which was not certified by peer review) is the author/funder, who has granted bioRxiv a license to display the preprint in perpetuity. It is made available under aCC-BY-NC-ND 4.0 International license.

QS regulates transcription of the *V. cholerae* CBASS operon

To determine if QS regulation of CBASS was at the level of transcription induction, we first monitored the abundance of *capV* and *dncV* transcripts in cultures of *V. cholerae* C6706 over time using RT-qPCR. Three hours following inoculation and corresponding with ~ 0.6 OD_{600}, a culture density consistent with the transition from LCD to HCD (36), the abundance of each transcript abruptly increased ~8-fold relative to their initial levels and remained high for the duration of the experiment (Fig. 4A). Notably, the increased abundance of both *capV* and *dncV* transcripts three hours post inoculation precedes both the SMX-dependent detection of cGAMP in the Δ*capV* mutant and growth inhibition by SMXof quorum fluent strains in previous experiments (Figs. 3A, 3B, S3A).

To confirm the observed increase in *capV* and *dncV* transcripts were the result of HCD gene expression we measured their abundance in a strain of C6706 (Δ*csqA*Δ*luxS*) (37) which is incapable of producing the two primary *V. cholerae* AIs, CAI-2 and AI-1. In monoculture, Δ*csqA*Δ*luxS* is locked in LCD gene expression, regardless of the population density, but can be converted to HCD gene expression by the introduction of exogenous AIs. Using RT-qPCR, we found when Δ*csqA*Δ*luxS* was grown in the presence of exogenous AIs there was at least a 6-fold greater abundance of *capV* and *dncV* transcripts than when grown in their absence (Fig. 4B). As a control, the abundance of *hapR* transcript also increased upon AI addition indicating the cultures had been converted to HCD gene expression (Fig. 4B).

bioRxiv preprint doi: https://doi.org/10.1101/2023.04.04.535582; this version posted April 4, 2023. The copyright holder for this preprint (which was not certified by peer review) is the author/funder, who has granted bioRxiv a license to display the preprint in perpetuity. It is made available under aCC-BY-NC-ND 4.0 International license.

To better understand how QS was regulating the abundance of CBASS transcripts, we constructed a luminescent transcriptional plasmid reporter containing a 913 nt region 5' of the *capV* translational start site with the CBASS promoter (pP_{CBASS}::*lux*) and measured luminescence generated by biofilm-null Δ*vpsL* QS mutants at LCD and HCD. The HCD-locked strain, Δ*vpsL*Δ*luxO* was the most luminescent at both densities whereas the LCD-locked strain, Δ*vpsL*Δ*hapR*, was sparingly luminescent regardless of the culture density (Fig. 4C). The quorum fluent strain, Δ*vpsL*, resembled Δ*vpsL*Δ*hapR* at LCD and Δ*vpsL*Δ*luxO* at HCD (Fig. 4C). These results indicated that transcription initiation of the CBASS promoter is positively regulated at HCD.

The transcription factor primarily responsible for HCD gene expression in *V. cholerae* is HapR (28). To determine if HapR could enhance expression of the CBASS promoter independent of additional *V. cholerae* genes, we measured the luminescent output of pP_{CBASS}::*lux* in a heterologous *E. coli* host and provided *hapR* in trans on an inducible plasmid (pHapR). The relative luminescence of *E. coli* cultures maintaining pHapR were significantly greater than the vector control following introduction of the inducer (Fig. 4D). In total, our data indicate CBASS is expressed as part of the HCD regulon in *V. cholerae* C6706 and this expression is induced by HapR.

HapR-dependent induction of CBASS transcription contributes to phage defense

QS induction of the CBASS operon suggests that this system would exhibit higher levels of phage defense at HCD. However, we have not identified a condition in which the *V. cholerae* CBASS operon protects against infection by the three major *V. cholerae* lytic phage ICP-1, ICP-2, and

bioRxiv preprint doi: https://doi.org/10.1101/2023.04.04.535582; this version posted April 4, 2023. The copyright holder for this preprint (which was not certified by peer review) is the author/funder, who has granted bioRxiv a license to display the preprint in perpetuity. It is made available under aCC-BY-NC-ND 4.0 International license.

283 ICP-3 (38). Thus, we are unable to test this prediction in *V. cholerae* expressing CBASS from its
284 native genomic context. To circumvent this challenge, we examined if the *V. cholerae* CBASS
285 operon provided phage defense when expressed from a low-copy cosmid (pVSP-1) in *E. coli* to
286 the lytic phage T2 in shaking liquid cultures. In these conditions, pVSP-1 alone provided only
287 minimal enhancement of *E. coli* growth when challenged with T2 at low multiplicities of
288 infection (MOIs) (Fig. 5A, S4). However, HapR expression substantially enhanced protection by
289 pVSP-1 to T2 phage infection, demonstrating that QS enhancement of CBASS expression leads
290 to greater phage defense (Fig. 5A, S4).
291
292 **Discussion**
293 The earliest strains of the El Tor biotype were first encountered during the period of 1897 –
294 1938 and considered non-pathogenic enteric commensals (3). Through genotypic analysis of
295 early and modern El Tor strains, Hu *et al.* (3) traced the evolutionary linage of the El Tor biotype
296 from non-pathogenic commensal to pandemic scourge in six phases. While these phases
297 include the predictable acquisition of key virulence factors including *tcpA*, *toxT*, and cholera
298 toxin, the 5th stage (1925-1954) is primarily defined by El Tor's acquisition of VSP-1 and -2 from
299 unknown origins. While it has been hypothesized that acquisition of VSP-1 and -2 potentiated El
300 Tor's pandemicity and rise to global dominance in the 7th Pandemic, we are just beginning to
301 understand their utility and the functions they encode.
302
303 Our analyses show that VSP-1 and -2 do not contribute to previously identified metabolic
304 differences between El Tor and Classical biotypes nor do they collectively influence colonization

bioRxiv preprint doi: https://doi.org/10.1101/2023.04.04.535582; this version posted April 4, 2023. The copyright holder for this preprint (which was not certified by peer review) is the author/funder, who has granted bioRxiv a license to display the preprint in perpetuity. It is made available under aCC-BY-NC-ND 4.0 International license.

in an infant mouse infection model. Rather, we demonstrate that the increased sensitivity to the antibiotic SMX in the model El Tor strain C6706 is due to the spurious activation of the abortive infection anti-phage Type-II CBASS encoded on VSP-1. Upon exposure to SMX, inhibition of folate biosynthesis de-represses DncV which leads to the synthesis of cGAMP (Fig. 5B). This increase of intracellular cGAMP allosterically activates the phospholipase CapV leading to the degradation of bacterial membranes and cell death (10) (Fig. 5B). We note that a recent study independently reached the same conclusion finding that the CBASS system of *V. cholerae* strain N16961 drove sensitivity to SMX (39). N16961 is a natural locked LCD mutant of *V. cholerae* with a non-functional *hapR,* and thus the role of QS in CBASS activity could not be observed in this study. In response to increased usage of SMX to treat cholera infections, SMX resistance has been observed in 79% of O1/O139 isolates (40). However, such resistance is not due to the loss of CBASS function but rather the acquisition of other resistance mechanisms like the SXT integrative conjugative element (41, 42). The fact that El Tor strains retain CBASS function and VSP-1 while acquiring resistance to SMX via alternate mechanisms argues that the VSP-1 island continues to play an important role in the fitness of circulating El Tor biotype strains. One such role could be enhanced resistance to phage predation which has been hypothesized to contributed to the global rise of the El Tor biotype and displacement of the classical biotype prior to the 7^{th} pandemic (43).

The link between SMX exposure and the activation of the VSP-1 CBASS is likely the result of non-competitive inhibition of DncV by folate molecules. The x-ray crystal structure of DncV unexpectedly revealed a molecule of 5-methyl-tetrahydrate folate bound on the opposite face

bioRxiv preprint doi: https://doi.org/10.1101/2023.04.04.535582; this version posted April 4, 2023. The copyright holder for this preprint (which was not certified by peer review) is the author/funder, who has granted bioRxiv a license to display the preprint in perpetuity. It is made available under aCC-BY-NC-ND 4.0 International license.

of the active site (34). Further study revealed that the in vitro cyclase activity of purified DncV was inhibited by the addition of various folate molecules (34). Additionally, introduction of the folate biosynthesis inhibitors sulfonamide and trimethoprim to *E. coli* expressing recombinant DncV led to an increase in the intracellular concentration of cGAMP relative to untreated cells (34). DncV belongs to the CD-NTase family of cyclic oligo-nucleotide synthases, which are often allosterically regulated (reviewed in (44)). For example, metazoan cGAS only synthesizes 2'3' cyclic GMP-AMP when bound to dsDNA as this is a biological signal for viral invasion or genome instability (45, 46) while the homolog cGLR1 from *Drosophila melanogaster* responds to dsRNA (47). Activation of DncV in *V. cholerae* by SMX indicates folates likely allosterically inhibit this CD-NTase in its native host.

Given that DncV initiates an abortive infection program (48), and its activity is inhibited by folates (34), we hypothesize that disruption of folate metabolism is a cellular indication of phage infection. In support of this idea, phage often encode nucleotide biosynthetic enzymes and extensively remodel cellular nucleotide pools, which can in turn alter folate metabolism. For example, the bacteriophage T4 encoded protein 55.1 forms a complex with *E. coli* FolD, a bifunctional enzyme that catalyzes interconversion of 5,10-methylene-tetrahydrofolate and 10-formyl-tetrahydrofolate, and induces hypersensitivity to trimethoprim (49). Additionally, the T4 strain, T4D, has been shown to shift the metabolism of folate compounds during infection in *E. coli* (reviewed in (50)). T4 phage have also been shown in numerous studies to be susceptible to CBASS anti-phage activities (11–13). Our results support a model (Fig. 5B) that depletion of folates upon phage infection is the activation signal for DncV to initiate abortive infection,

bioRxiv preprint doi: https://doi.org/10.1101/2023.04.04.535582; this version posted April 4, 2023. The copyright holder for this preprint (which was not certified by peer review) is the author/funder, who has granted bioRxiv a license to display the preprint in perpetuity. It is made available under aCC-BY-NC-ND 4.0 International license.

349 though this remains to be formally tested. It is also unclear whether folates facilitate or
350 antagonize the dichotomous activities of Cap2 and Cap3 which enhance and suppress DncV
351 activity, respectively, through post-translation modification of its C-terminus (12, 13). Under the
352 conditions we tested, activation by folate depletion is indifferent to the post-translational
353 modification state of DncV as loss of either *cap2* or *cap3* did not substantially affect SMX
354 sensitivity (Figs. 2D & S2F).
355
356 Our studies of SMX activation of DncV showed a consistent delay in cell killing, which we
357 determined is due to the QS-dependent transcription of CBASS by the HCD transcriptional
358 regulator HapR (Fig. 5B). In agreement with this, RNA-seq analysis of *V. cholerae* C6706
359 demonstrated that CBASS transcripts were significantly more abundant at HCD than LCD (22).
360 QS regulation appears to be another mechanism to restrict the activity of the VSP-1 CBASS
361 system to the most appropriate conditions, thereby preventing spurious activation of DncV and
362 CapV and unnecessary cell death. Identification of the VSP-1 encoded transcription factor VspR
363 (Fig. 2C, 5B) was pivotal to the discovery of DncV (18). ChIP analysis revealed VspR was
364 associated with DNA sequences found within the CBASS locus and *vspR* mutants contained a
365 greater abundance of CBASS gene transcripts, implicating it as a negative transcriptional
366 regulator of CBASS (18). Contrary to our expectation, under our experimental conditions *vspR*
367 did not contribute to CBASS-dependent SMX sensitivity (Fig. 2D & S2F). If and how VspR and QS
368 regulation of CBASS overlap remains to be explored.
369

bioRxiv preprint doi: https://doi.org/10.1101/2023.04.04.535582; this version posted April 4, 2023. The copyright holder for this preprint (which was not certified by peer review) is the author/funder, who has granted bioRxiv a license to display the preprint in perpetuity. It is made available under aCC-BY-NC-ND 4.0 International license.

The role of QS in defense against phage has been previously described (reviewed in (51)) and some notable examples include the regulation of phage receptor abundance in *E. coli* (52) as well as haemaglutinin protease production in El Tor *V. cholerae* (53), CRISPR-Cas expression in *Pseudomonas aeruginosa* (54), and the *hapR* independent HCD-regulation of the El Tor VSP-II encoded *ddmABC* anti-phage and plasmid defense system (15). From an ecological perspective, reserving the expression and activity of the VSP-1 CBASS to situations where El Tor *V. cholerae* would find itself in an environment densely populated with kin fits with its biological function of preventing phage infection by abortive replication. HCD populations are environments where phage will be the most prevalent and bacteria at greater risk of infection. At LCD, when neighbors are scarce, abortive infection is unlikely to be an evolutionarily advantageous strategy and infected cells may instead rely on non-lethal phage defense mechanisms. Though this remains to be formally tested, one scenario in which El Tor *Vibrio cholerae* defends against phage could be a reliance of the non-lethal depletion of nucleotides by the *avcID* system (8, 9) at LCD and the CBASS system at HCD, both of which are encoded in VSP-1. Although the molecular mechanism of CBASS are now well characterized (55), the regulation of such systems and their contribution to bacterial evolution and environmental adaptation is just beginning to be described. CBASS are widely conserved in bacteria (19) and whether QS regulation of such systems is commonplace should be further investigated.

References

1. Clemens JD, Nair GB, Ahmed T, Qadri F, Holmgren J. 2017. Cholera. Lancet (London, England) 390:1539–1549.
2. Siddique AK, Cash R. 2014. Cholera outbreaks in the classical biotype era. Curr Top Microbiol Immunol 379:1–16.

bioRxiv preprint doi: https://doi.org/10.1101/2023.04.04.535582; this version posted April 4, 2023. The copyright holder for this preprint (which was not certified by peer review) is the author/funder, who has granted bioRxiv a license to display the preprint in perpetuity. It is made available under aCC-BY-NC-ND 4.0 International license.

3. Hu D, Liu B, Feng L, Ding P, Guo X, Wang M, Cao B, Reeves PR, Wang L. 2016. Origins of the current seventh cholera pandemic. Proc Natl Acad Sci U S A 113:E7730–E7739.
4. Son MS, Taylor RK. 2011. Genetic Screens and Biochemical Assays to Characterize Vibrio cholerae O1 Biotypes: Classical and El Tor. Curr Protoc Microbiol 22A:6A.2.1-6A.2.17.
5. Northrup RS, Doyle MA, Feeley JC. 1972. In vitro susceptibility of El Tor and classical Vibrio cholerae strains to trimethoprim and sulfamethoxazole. Antimicrob Agents Chemother 1:310–4.
6. Dziejman M, Balon E, Boyd D, Fraser CM, Heidelberg JF, Mekalanos JJ. 2002. Comparative genomic analysis of Vibrio cholerae: Genes that correlate with cholera endemic and pandemic disease. Proc Natl Acad Sci U S A 99:1556–1561.
7. O'Shea YA, Finnan S, Reen FJ, Morrissey JP, O'Gara F, Boyd EF. 2004. The Vibrio seventh pandemic island-II is a 26·9 kb genomic island present in Vibrio cholerae El Tor and O139 serogroup isolates that shows homology to a 43·4 kb genomic island in V. vulnificus. Microbiology 150:4053–4063.
8. Hsueh BY, Severin GB, Elg CA, Waldron EJ, Kant A, Wessel AJ, Dover JA, Rhoades CR, Ridenhour BJ, Parent KN, Neiditch MB, Ravi J, Top EM, Waters CM. 2022. Phage defence by deaminase-mediated depletion of deoxynucleotides in bacteria. Nat Microbiol 7:1210–1220.
9. Tal N, Millman A, Stokar-Avihail A, Fedorenko T, Leavitt A, Melamed S, Yirmiya E, Avraham C, Brandis A, Mehlman T, Amitai G, Sorek R. 2022. Bacteria deplete deoxynucleotides to defend against bacteriophage infection. Nat Microbiol 7:1200–1209.
10. Severin GB, Ramliden MS, Hawver LA, Wang K, Pell ME, Kieninger A-K, Khataokar A, O'Hara BJ, Behrmann L V., Neiditch MB, Benning C, Waters CM, Ng W-L. 2018. Direct activation of a phospholipase by cyclic GMP-AMP in El Tor Vibrio cholerae. Proc Natl Acad Sci U S A 115:E6048–E6055.
11. Cohen D, Melamed S, Millman A, Shulman G, Oppenheimer-Shaanan Y, Kacen A, Doron S, Amitai G, Sorek R. 2019. Cyclic GMP-AMP signalling protects bacteria against viral infection. Nature 574:691–695.
12. Ledvina HE, Ye Q, Gu Y, Sullivan AE, Quan Y, Lau RK, Zhou H, Corbett KD, Whiteley AT. 2023. An E1–E2 fusion protein primes antiviral immune signalling in bacteria. Nature. doi: 10.1038/s41586-022-05647-4
13. Jenson JM, Li T, Du F, Ea C-K, Chen ZJ. 2023. Ubiquitin-like Conjugation by Bacterial cGAS Enhances Anti-phage Defence. Nature https://doi.org/10.1038/s41586-023-05862-7.
14. Jaskólska M, Adams DW, Blokesch M. 2022. Two defence systems eliminate plasmids from seventh pandemic Vibrio cholerae. Nature 604:323–329.
15. O'Hara BJ, Alam M, Ng W-L. 2022. The Vibrio cholerae Seventh Pandemic Islands act in tandem to defend against a circulating phage. PLoS Genet 18:e1010250.
16. Murphy SG, Johnson BA, Ledoux CM, Dörr T. 2021. Vibrio cholerae's mysterious Seventh Pandemic island (VSP-II) encodes novel Zur-regulated zinc starvation genes involved in chemotaxis and cell congregation. PLoS Genet 17:e1009624.
17. Whiteley AT, Eaglesham JB, de Oliveira Mann CC, Morehouse BR, Lowey B, Nieminen EA, Danilchanka O, King DS, Lee ASY, Mekalanos JJ, Kranzusch PJ. 2019. Bacterial cGAS-like enzymes synthesize diverse nucleotide signals. Nature 567:194–199.
18. Davies BW, Bogard RW, Young TS, Mekalanos JJ. 2012. Coordinated regulation of

bioRxiv preprint doi: https://doi.org/10.1101/2023.04.04.535582; this version posted April 4, 2023. The copyright holder for this preprint (which was not certified by peer review) is the author/funder, who has granted bioRxiv a license to display the preprint in perpetuity. It is made available under aCC-BY-NC-ND 4.0 International license.

accessory genetic elements produces cyclic di-nucleotides for V. cholerae virulence. Cell 149:358–70.

19. Millman A, Melamed S, Amitai G, Sorek R. 2020. Diversity and classification of cyclic-oligonucleotide-based anti-phage signalling systems. Nat Microbiol 5:1608–1615.
20. Ng W-L, Bassler BL. 2009. Bacterial quorum-sensing network architectures. Annu Rev Genet 43:197–222.
21. Papenfort K, Bassler BL. 2016. Quorum sensing signal-response systems in Gram-negative bacteria. Nat Rev Microbiol 14:576–88.
22. Papenfort K, Förstner KU, Cong J-P, Sharma CM, Bassler BL. 2015. Differential RNA-seq of Vibrio cholerae identifies the VqmR small RNA as a regulator of biofilm formation. Proc Natl Acad Sci U S A 112:E766-75.
23. Herrington DA, Hall RH, Losonsky G, Mekalanos JJ, Taylor RK, Levine MM. 1988. Toxin, toxin-coregulated pili, and the toxR regulon are essential for Vibrio cholerae pathogenesis in humans. J Exp Med 168:1487–92.
24. Thelin KH, Taylor RK. 1996. Toxin-coregulated pilus, but not mannose-sensitive hemagglutinin, is required for colonization by Vibrio cholerae O1 El Tor biotype and O139 strains. Infect Immun 64:2853–6.
25. Brumfield KD, Carignan BM, Ray JN, Jumpre PE, Son MS. 2017. Laboratory Techniques Used to Maintain and Differentiate Biotypes of Vibrio cholerae Clinical and Environmental Isolates. J Vis Exp https://doi.org/10.3791/55760.
26. Yoon SS, Mekalanos JJ. 2006. 2,3-butanediol synthesis and the emergence of the Vibrio cholerae El Tor biotype. Infect Immun 74:6547–56.
27. Hawver LA, Giulietti JM, Baleja JD, Ng W-L. 2016. Quorum Sensing Coordinates Cooperative Expression of Pyruvate Metabolism Genes To Maintain a Sustainable Environment for Population Stability. MBio 7.
28. Zhu J, Miller MB, Vance RE, Dziejman M, Bassler BL, Mekalanos JJ. 2002. Quorum-sensing regulators control virulence gene expression in Vibrio cholerae. Proc Natl Acad Sci U S A 99:3129–34.
29. DiRita VJ, Neely M, Taylor RK, Bruss PM. 1996. Differential expression of the ToxR regulon in classical and E1 Tor biotypes of Vibrio cholerae is due to biotype-specific control over toxT expression. Proc Natl Acad Sci U S A 93:7991–7995.
30. Kaper JB, Morris JG, Levine MM. 1995. Cholera. Clin Microbiol Rev 8:48–86.
31. Stutzmann S, Blokesch M. 2016. Circulation of a Quorum-Sensing-Impaired Variant of Vibrio cholerae Strain C6706 Masks Important Phenotypes. mSphere 1:1–10.
32. Hankins J V, Madsen JA, Giles DK, Brodbelt JS, Trent MS. 2012. Amino acid addition to Vibrio cholerae LPS establishes a link between surface remodeling in gram-positive and gram-negative bacteria. Proc Natl Acad Sci U S A 109:8722–7.
33. Matson JS, Yoo HJ, Hakansson K, Dirita VJ. 2010. Polymyxin B resistance in El Tor Vibrio cholerae requires lipid acylation catalyzed by MsbB. J Bacteriol 192:2044–52.
34. Zhu D, Wang L, Shang G, Liu X, Zhu J, Lu D, Wang L, Kan B, Zhang J-R, Xiang Y. 2014. Structural biochemistry of a Vibrio cholerae dinucleotide cyclase reveals cyclase activity regulation by folates. Mol Cell 55:931–937.
35. Waters CM, Lu W, Rabinowitz JD, Bassler BL. 2008. Quorum sensing controls biofilm formation in Vibrio cholerae through modulation of cyclic di-GMP levels and repression

bioRxiv preprint doi: https://doi.org/10.1101/2023.04.04.535582; this version posted April 4, 2023. The copyright holder for this preprint (which was not certified by peer review) is the author/funder, who has granted bioRxiv a license to display the preprint in perpetuity. It is made available under aCC-BY-NC-ND 4.0 International license.

of vpsT. J Bacteriol 190:2527–36.
36. Miller MB, Skorupski K, Lenz DH, Taylor RK, Bassler BL. 2002. Parallel quorum sensing systems converge to regulate virulence in Vibrio cholerae. Cell 110:303–14.
37. Hammer BK, Bassler BL. 2007. Regulatory small RNAs circumvent the conventional quorum sensing pathway in pandemic Vibrio cholerae. Proc Natl Acad Sci U S A 104:11145–9.
38. Seed KD, Bodi KL, Kropinski AM, Ackermann H-W, Calderwood SB, Qadri F, Camilli A. 2011. Evidence of a Dominant Lineage of Vibrio cholerae-Specific Lytic Bacteriophages Shed by Cholera Patients over a 10-Year Period in Dhaka, Bangladesh. MBio 2:e00334-10.
39. Brenzinger S, Airoldi M, Ogunleye AJ, Brochado AR. 2023. The antiphage defense system CBASS controls resistance and enables killing by antifolate antibiotics in Vibrio cholerae bioRxiv 2023.02.27.530311.
40. Liu C, Wang Y, Azizian K, Omidi N, Hassan Kaviar V, Kouhsari E, Maleki A. 2022. Antimicrobial resistance in Vibrio cholerae O1/O139 clinical isolates: a systematic review and meta-analysis. Expert Rev Anti Infect Ther 20:1217–1231.
41. Wozniak RAF, Fouts DE, Spagnoletti M, Colombo MM, Ceccarelli D, Garriss G, Déry C, Burrus V, Waldor MK. 2009. Comparative ICE genomics: insights into the evolution of the SXT/R391 family of ICEs. PLoS Genet 5:e1000786.
42. Bhotra T, Das MM, Pal BB, Singh D V. 2016. Genomic profile of antibiotic resistant, classical ctxB positive Vibrio cholerae O1 biotype El Tor isolated in 2003 and 2005 from Puri, India: A retrospective study. Indian J Med Microbiol 34:462–470.
43. Zahid MSH, Waise Z, Kamruzzaman M, Ghosh AN, Nair GB, Khairul Bashar SAM, Mekalanos JJ, Faruque SM. 2011. An experimental study of phage mediated bactericidal selection & emergence of the El Tor Vibrio cholerae. Indian J Med Res 133:218–24.
44. Kranzusch PJ. 2019. cGAS and CD-NTase enzymes: structure, mechanism, and evolution. Curr Opin Struct Biol 59:178–187.
45. Gao P, Ascano M, Wu Y, Barchet W, Gaffney BL, Zillinger T, Serganov AA, Liu Y, Jones RA, Hartmann G, Tuschl T, Patel DJ. 2013. Cyclic [G(2',5')pA(3',5')p] is the metazoan second messenger produced by DNA-activated cyclic GMP-AMP synthase. Cell 153:1094–107.
46. Civril F, Deimling T, de Oliveira Mann CC, Ablasser A, Moldt M, Witte G, Hornung V, Hopfner K-P. 2013. Structural mechanism of cytosolic DNA sensing by cGAS. Nature 498:332–7.
47. Hartmann R, Justesen J, Sarkar SN, Sen GC, Yee VC. 2003. Crystal structure of the 2'-specific and double-stranded RNA-activated interferon-induced antiviral protein 2'-5'-oligoadenylate synthetase. Mol Cell 12:1173–85.
48. Cohen D, Melamed S, Millman A, Shulman G, Oppenheimer-Shaanan Y, Kacen A, Doron S, Amitai G, Sorek R. 2019. Cyclic GMP-AMP signalling protects bacteria against viral infection. Nature 574:691–695.
49. Mattenberger Y, Mattson S, Métrailler J, Silva F, Belin D. 2011. 55.1, a gene of unknown function of phage T4, impacts on Escherichia coli folate metabolism and blocks DNA repair by the NER. Mol Microbiol 82:1406–21.
50. Green JM, Matthews RG. 2007. Folate Biosynthesis, Reduction, and Polyglutamylation and the Interconversion of Folate Derivatives. EcoSal Plus 2.
51. Wang Y, Dai J, Wang X, Wang Y, Tang F. 2022. Mechanisms of interactions between

bioRxiv preprint doi: https://doi.org/10.1101/2023.04.04.535582; this version posted April 4, 2023. The copyright holder for this preprint (which was not certified by peer review) is the author/funder, who has granted bioRxiv a license to display the preprint in perpetuity. It is made available under aCC-BY-NC-ND 4.0 International license.

bacteria and bacteriophage mediate by quorum sensing systems. Appl Microbiol Biotechnol 106:2299–2310.

52. Høyland-Kroghsbo NM, Maerkedahl RB, Svenningsen S Lo. 2013. A quorum-sensing-induced bacteriophage defense mechanism. MBio 4:e00362-12.

53. Hoque MM, Naser I Bin, Bari SMN, Zhu J, Mekalanos JJ, Faruque SM. 2016. Quorum Regulated Resistance of Vibrio cholerae against Environmental Bacteriophages. Sci Rep 6:37956.

54. Høyland-Kroghsbo NM, Paczkowski J, Mukherjee S, Broniewski J, Westra E, Bondy-Denomy J, Bassler BL. 2017. Quorum sensing controls the Pseudomonas aeruginosa CRISPR-Cas adaptive immune system. Proc Natl Acad Sci U S A 114:131–135.

55. Duncan-Lowey B, Kranzusch PJ. 2022. CBASS phage defense and evolution of antiviral nucleotide signaling. Curr Opin Immunol 74:156–163.

56. Skorupski K, Taylor RK. 1996. Positive selection vectors for allelic exchange. Gene 169:47–52.

57. Lenz DH, Miller MB, Zhu J, Kulkarni R V, Bassler BL. 2005. CsrA and three redundant small RNAs regulate quorum sensing in Vibrio cholerae. Mol Microbiol 58:1186–202.

58. Gerhardt P, Murray R. E, Wood WA, Krieg NR. 1994. Methods for General and Molecular Bacteriology, 1st ed. American Society for Microbiology, Washington, D. C.

59. Van Alst AJ, DiRita VJ. 2020. Aerobic Metabolism in Vibrio cholerae Is Required for Population Expansion during Infection. MBio 11.

60. Anthouard R, DiRita VJ. 2013. Small-Molecule Inhibitors of toxT Expression in Vibrio cholerae. MBio 4.

61. Massie JP, Reynolds EL, Koestler BJ, Cong J-P, Agostoni M, Waters CM. 2012. Quantification of high-specificity cyclic diguanylate signaling. Proc Natl Acad Sci 109:12746–12751.

62. Dunn AK, Millikan DS, Adin DM, Bose JL, Stabb E V. 2006. New rfp- and pES213-derived tools for analyzing symbiotic Vibrio fischeri reveal patterns of infection and lux expression in situ. Appl Environ Microbiol 72:802–10.

63. Svenningsen SL, Waters CM, Bassler BL. 2008. A negative feedback loop involving small RNAs accelerates Vibrio cholerae's transition out of quorum-sensing mode. Genes Dev 22:226–38.

64. Friedman AM, Long SR, Brown SE, Buikema WJ, Ausubel FM. 1982. Construction of a broad host range cosmid cloning vector and its use in the genetic analysis of Rhizobium mutants. Gene 18:289–96.

bioRxiv preprint doi: https://doi.org/10.1101/2023.04.04.535582; this version posted April 4, 2023. The copyright holder for this preprint (which was not certified by peer review) is the author/funder, who has granted bioRxiv a license to display the preprint in perpetuity. It is made available under aCC-BY-NC-ND 4.0 International license.

Materials and Methods

Growth conditions and media:

All strains of *V. cholerae* and *E. coli* were grown in LB broth-Miller media (NEOGEN) at 35° C with aeration, unless otherwise stated. When noted, antibiotic selection was utilized at the following concentrations: streptomycin (50 µg/mL), chloramphenicol (10 µg/mL when used alone or 5 µg/mL when used with another antibiotic), kanamycin (100 µg/mL when used alone; 50 µg/mL when used with another antibiotic) and tetracycline (5 µg/mL). IPTG was used at 6.25-10 µM as indicated. *E. coli* BW29427, a diaminopimelic acid (DAP) auxotroph, was additionally supplemented with 300 µg/mL DAP and used for the conjugative transfer of vectors and cosmids to all *V. cholerae* strains presented in this work.

Cloning and strain construction:

All gene deletions from the *V. cholerae* genome were performed using the vector pKAS32 (56). Deletion constructs were cloned using a three-piece Gibson Assembly composed of ~1 kb homologous sequences both 5' and 3' of the genomic region to be removed and linear pKAS32 double digested with KpnI and SacI. Mutants were obtained through allelic exchange (56) and verified by Sanger sequencing. All mutants utilized in this study were complete deletions of the genomic regions of interest except for Δ*vspR* where the *vspR* codons 1, 2, and 6 where all mutated into stop codons. The pP_{CBASS}::*lux* plasmid was generated by amplification of 913 n.t. upstream of *capV* and Gibson assembly into BamHI/SpeI digested pBBR-lux (57) using the primers Lux_CBASSpr_FW and Lux_CBASSpr_RV, 5'.

bioRxiv preprint doi: https://doi.org/10.1101/2023.04.04.535582; this version posted April 4, 2023. The copyright holder for this preprint (which was not certified by peer review) is the author/funder, who has granted bioRxiv a license to display the preprint in perpetuity. It is made available under aCC-BY-NC-ND 4.0 International license.

583 **Metabolic Growth Assays**

584 Using an inoculating loop, overnight cultures were applied as a single streak on the
585 surface of agar plates and incubated at 35° C for 24 h. Images were taken of plates using an
586 iPhone. For the casein hydrolysis protease assay, milk agar plates were prepared according to (4)
587 and contained 20.0 g/L dry skim milk and 9.2 g/L brain-heart infusion and 15 g/L agar. Blood
588 agar plates were prepared according to (58) using Mueller Hinton Broth in 1.5% agar with 5%
589 sheep blood. Citrate minimal medium agar was prepared according to (4). For comparing
590 growth on MacConkey agar, an overnight culture of each strain was normalized to an OD_{600} of
591 0.5 and serial diluted ten-fold in PBS to 10^{-7}. 2.5 µl of each dilution was plated on both LB and
592 MacConkey agar plates and incubated ~16 h at 35° C and imaged with an iPhone. For the Voges-
593 Proskauer (VP) Assay, each strain was inoculated in 3 mL of Methyl Red - Voges-Proskauer (MR-
594 VP) broth medium (4) from a plate and incubated overnight. Then, 130 µL of 5% (w/v) α-
595 naphthol and 43 µl of 1M potassium hydroxide was added to 1mL aliquots of the overnight
596 cultures and allowed color to develop over 48 h at room temperature.
597
598 **Infant Mouse Competition Assay**

599 Infant mice were infected as described previously (59, 60). Briefly, three- to five- day old
600 CD-1 neonate mice (Charles River, Wilmington, MA) were orogastrically inoculated with
601 approximately 10^6 total CFU 2 h after separation from dam mice. ΔVSP-1/2 was co-inoculated
602 1:1 with a Δ*lacZ* C6706str2 strain to allow for differentiation by blue-white screening upon
603 recovery. Mice were maintained at 30°C until euthanasia 20 h post inoculation. To enumerate *V.*
604 *cholerae* CFU, intestinal segments (small intestine and the large intestine plus cecum) were

bioRxiv preprint doi: https://doi.org/10.1101/2023.04.04.535582; this version posted April 4, 2023. The copyright holder for this preprint (which was not certified by peer review) is the author/funder, who has granted bioRxiv a license to display the preprint in perpetuity. It is made available under aCC-BY-NC-ND 4.0 International license.

homogenized, serially diluted, and plated on LB + 0.1 mg/mL streptomycin, 0.08 mg/mL 5-bromo-4-chloro-3-indolyl-β-D-galactopyranoside (X-Gal). Blue and white colony counts were used to determine the competitive index (C.I.) for ΔVSP-1/2 using the following equation: C.I. = (CFU ΔVSP-1/2$_{intestine}$ / CFU Δ*lacZ*$_{intestine}$)/(CFU ΔVSP-1/2$_{inoculum}$ / CFU Δ*lacZ*$_{inoculum}$). The fitness of the Δ*lacZ* strain was previously shown to have no colonization defect relative to the parental C6706str2 (59). All animal experiments in this study were approved by the Institutional Animal Care and Use Committee at Michigan State University.

Polymyxin B IC_{50}

For the polymyxin B resistance assay, 2 mL LB cultures were incubated for 16 h at 35° C with aeration. Cultures were then diluted 1:100 in fresh LB, aliquoted into 96-well plates (COSTAR), and challenged with a four-fold serial dilution of polymyxin B (Sigma) from 55.5 µg/mL to 0.014 µg/mL. Plates were incubated for 20 h without aeration at 35° C and the culture absorbance was measured at 600 nm using an Envision 2105 Multimode Plate Reader (Perkin-Elmer) and % growth for each biological replicate was calculated by dividing the absorbance 600 nm of polymyxin B treated wells by the absorbance of the untreated control well. The reported mean % growth and standard deviation were calculated from three biological replicates for each polymyxin B concentration. IC_{50} were calculated using a non-linear regression analysis performed using GraphPad Prism version 9.5.0.

Sulfamethoxazole IC_{50} and Challenges

bioRxiv preprint doi: https://doi.org/10.1101/2023.04.04.535582; this version posted April 4, 2023. The copyright holder for this preprint (which was not certified by peer review) is the author/funder, who has granted bioRxiv a license to display the preprint in perpetuity. It is made available under aCC-BY-NC-ND 4.0 International license.

Overnight cultures were grown in the presence of streptomycin unless pLAFR derived cosmids were being maintained, in which case tetracycline was supplemented in place of streptomycin. Sulfamethoxazole (10 mg/mL) stocks were prepared in DMSO, diluted in LB to concentrations 15 x greater than the final desired concentration, and multichannel pipetted into clear polystyrene 96-well plates (COSTAR) in 10 µL aliquots. Overnight cultures were diluted 1:10,000 in fresh media supplemented with the same antibiotic selection as the overnight media. One hundred and forty µL of the diluted cultures were multichannel pipetted into 96-well plates preloaded with trimethoprim or sulfamethoxazole. Plates were wrapped in parafilm and incubated at 35° C with aeration for 24 h. Culture absorbance was measured at 600 nm using an Envision 2105 Multimode Plate Reader (Perkin-Elmer). % growth for each biological replicate was calculated by dividing the mean absorbance of technical replicate treatment wells (N = 2 to 4) by the mean absorbance of technical replicate untreated control wells (N = 2 to 4). The reported mean % growth and standard error mean were calculated from three biological replicates for each concentration. IC_{50} were calculated using a non-linear regression analysis performed using GraphPad Prism version 9.5.0.

Growth curves and cGAMP quantification by UPLC-MS/MS following Sulfamethoxazole challenge

Overnight cultures were started in triplicate from freezer stocks and grown in LB supplemented with streptomycin. Cultures were inoculated 1:1,000 in 50 mL fresh media containing selection in 125 mL flasks and grown for 15 minutes before being divided equally into two sister cultures. Sister cultures were grown for one additional hour before being

bioRxiv preprint doi: https://doi.org/10.1101/2023.04.04.535582; this version posted April 4, 2023. The copyright holder for this preprint (which was not certified by peer review) is the author/funder, who has granted bioRxiv a license to display the preprint in perpetuity. It is made available under aCC-BY-NC-ND 4.0 International license.

sampled to assess culture growth by measuring absorbances at 600 nm and CFU enumeration by serial dilution plating. Immediately following the initial sampling, sister cultures were challenged with either 100 µg/mL SMX or a DMSO vehicle control and further sampling continued at ~30 minute intervals for the duration of the experiment. We elected to challenge these strains with 100 µg/mL SMX as this was sufficient to induce CBASS dependent SMX sensitivity in C6706 and below the IC_{50} of ΔVSP-1 (Figs. 2A, S2A & Table S1), which has an analogous SMX resistance phenotype to the Δ*capV* strain (Figs. 2D & S2F).

For the purposes of measuring intracellular cGAMP additional aliquots of Δ*capV* sister cultures (+/- 100 µg/mL sulfamethoxazole) were removed at all time points during this experiment and similarly analyzed as previously described (10). One-milliliter culture aliquots were pelleted at 15k x g in microcentrifuge tubes for 1 minute, supernatants were removed by aspiration, and pelleted cells were suspended in 200 µL of ice-cold extraction buffer (acetonitrile, methanol, HPLC-grade water, formic acid (2:2:1:0.02, v/v/v/v)), and stored at -20° C overnight. Extracts were centrifugation at 15k x g for 1 minute, to remove cellular debris, and the resulting clarified extracts were transferred to new a microcentrifuge tube and dried in a SpeedVac. Desiccated extracts were dissolved in 100 µL of HPLC-grade water and loaded into glass sample vials for UPLC-MS/MS analysis using an Acquity Ultra Performance LC system (Waters) coupled with a Quattro Premier XE mass spectrometer (Waters). Chromatography and multiple reaction monitoring parameters performed as previously described (10). A cGAMP standard curve was generated using a two-fold serial dilution of cGAMP (Axxora) in HPLC-grade water spanning 1.9-125 nM. Intracellular concentrations of cGAMP were calculated by dividing

bioRxiv preprint doi: https://doi.org/10.1101/2023.04.04.535582; this version posted April 4, 2023. The copyright holder for this preprint (which was not certified by peer review) is the author/funder, who has granted bioRxiv a license to display the preprint in perpetuity. It is made available under aCC-BY-NC-ND 4.0 International license.

669 the total moles of cGAMP in a sample by the product of the enumerated CFU in each sample
670 and a standard cell volume of 6.46×10^{-16} L (10, 61).
671
672 **Growth curves of sulfamethoxazole treated quorum sensing and CBASS mutants**
673 Overnight cultures were diluted to an OD_{600} of 0.01 in 6 mL fresh LB medium, recovered
674 for 1h at 37° C with aeration, and split into paired test tubes. Within a pair of cultures, one was
675 challenged with 100 µg/mL sulfamethoxazole, dissolved in DMSO, while the second culture was
676 challenged with DMSO vehicle control. Cultures were incubated at 37° C with aeration and the
677 culture OD_{600} was measured at the times presented for the duration of each experiment. The
678 mean and standard deviation of biological triplicate samples for all strains and treatments is
679 reported.
680
681 **Time course gene expression using RT-qPCR**
682 Biological duplicate overnight cultures were started from freezer stock in LB and back
683 diluted 1:10,000 into 250 mL LB in 1 L flasks and grown at 35° C with aeration. Cultures were
684 sampled 2, 2.5, 3, 4, and 5 h post inoculation in 50, 30, 1, 0.5, and 0.5 mL aliquots, respectively,
685 and cells were pelleted by centrifugation. Cell pellets were suspended in 1 mL TRIzol™ Reagant
686 (Thermo Fischer) and RNA was purified following manufacturer's specifications. Following
687 manufacturer recommendations, 5 µg of RNA was treated with TURBO™ Dnase (Ambion) and
688 cDNA was generated using SuperScript™ III (Thermo Fischer). SYBR™ Green PCR Master Mix
689 (Thermo Fischer) was used according to the manufacture's recommendations in 25 µL reactions
690 containing 6.25 ng cDNA template (no reverse-transcription controls used 6.25 ng DNAse-

bioRxiv preprint doi: https://doi.org/10.1101/2023.04.04.535582; this version posted April 4, 2023. The copyright holder for this preprint (which was not certified by peer review) is the author/funder, who has granted bioRxiv a license to display the preprint in perpetuity. It is made available under aCC-BY-NC-ND 4.0 International license.

treated RNA template) and a final primer concentration of 100 nM. qRT-PCRs reactions were performed in technical duplicate using a StepOnePlus real-time PCR system (Thermo Fisher Scientific). Gene expression was calculated using ΔCT relative to the *gyrA* housekeeping gene and comparative ΔΔCT was determined by comparison of each time point to the ΔCT of the initial 2 h sample (~0.05 OD_{600}).

Gene expression in response to exogenous autoinducers by RT-qPCR

Colonies of Δ*csqA*Δ*luxS V. cholerae* were inoculated into LB and incubated with aeration at 30° C for 16 hours. Each culture was then diluted 1:500 – once into fresh LB supplemented autoinducers (5 µM CAI-1 and 5 µM AI-2) and once into fresh LB without autoinducers. These cultures were incubated with aeration at 30° C for 2 hours, at which point the OD_{600} measurements for all cultures were confirmed to be similar (OD_{600} = 0.4-0.45). Cells were lysed in TRIzol™ Reagent (Invitrogen) then RNA was extracted using the Direct-zol RNA Microprep kit (Zymo Research). RNA was then treated with 0.5 µl TURBO™ DNase (Invitrogen) at 37° C for 90 minutes, then an additional 0.5 µl TURBO™ DNAse was added and the samples were incubated for an additional 90 minutes at 37° C. cDNA was synthesized from total RNA using the SuperScript™ III Reverse Transcriptase kit (Invitrogen). For each sample, RT-qPCR was performed on 50 ng of cDNA using the SYBR™ Select Master Mix kit (Applied Biosystems) and 250 nM of each primer. Expression levels were calculated for each target gene by normalizing to the housekeeping gene *recA*, then the relative fold expression was calculated by comparing the target gene expression in the presence of autoinducers to the absence of autoinducers and reported as the mean of measurements obtained from three biological replicates.

bioRxiv preprint doi: https://doi.org/10.1101/2023.04.04.535582; this version posted April 4, 2023. The copyright holder for this preprint (which was not certified by peer review) is the author/funder, who has granted bioRxiv a license to display the preprint in perpetuity. It is made available under aCC-BY-NC-ND 4.0 International license.

Luminescent reporter assays

To assess QS induction of CBASS transcription, overnight cultures of Δ*vpsL*, Δ*vpsL*Δ*hapR*, and Δ*vpsL*Δ*luxO* (35) containing pP_{CBASS}::*lux* (pKAD1) inoculated from individual colonies (n=3) grown in LB in glass test tubes were back diluted 1:1,000 in 3 mLs of LB with chloramphenicol and grown with shaking at 35° C. At two hours, to measure low cell density, and 20 hours, to measure high cell density, the bioluminescence and OD_{600} of 200 mL of each culture was transferred to a solid black 96-well plate and quantified on an Envision 2105 Multimode Plate Reader (Perkin-Elmer). Relative light units were determined by dividing the bioluminescence by the OD_{600}, and each was normalized to the mean relative light units of the locked high cell density Δ*vpsL*Δ*luxO* mutant at the corresponding time point.

pHapR and pVSP-1 in E coli

Three independent 2 mL overnight cultures of *E. coli* DH10B with pP_{CBASS}::*lux* (pKAD1) with pVector2 (pEVS141) (62) or pHapR (pSLS13) (63) grown in LB with chloramphenicol (5 μg/mL) and kanamycin (50 μg/mL) were back diluted 1:100 in the same media. 150 μL of each culture was placed in a solid black 96-well plate and incubated without shaking at 35° C. After 1.5 hours, HapR production was induced with 6.25 μg/mL IPTG, and bioluminescence and OD600 were measured on an Envision 2105 Multimode Plate Reader (Perkin-Elmer) hourly.

Phage Challenge Assay

bioRxiv preprint doi: https://doi.org/10.1101/2023.04.04.535582; this version posted April 4, 2023. The copyright holder for this preprint (which was not certified by peer review) is the author/funder, who has granted bioRxiv a license to display the preprint in perpetuity. It is made available under aCC-BY-NC-ND 4.0 International license.

734 Overnight cultures of *E. coli* DH10B with pVector (pLAFR) (64) or pVSP-1 (10) combined with
735 pVector2 (pEVS141) (62) or pHapR (pSLS13) (63) were grown in 2 mL LB with 50 μg/mL
736 kanamycin and 5 μg/mL tetracycline overnight at 35° C with shaking. Each culture was back
737 diluted 1:1,000 in 2 mL of LB with the same antibiotics + 10 μM IPTG and grown 2-3 hours with
738 shaking at 35° C before addition of T2 phage at the indicated MOI followed by overnight growth
739 with shaking at 35° C. The OD_{600} was measured the following day (~20 hours) on an Envision
740 2105 Multimode Plate Reader (Perkin-Elmer), and the OD_{600} of each culture was normalized to
741 the uninfected control and reported as percent growth.
742

bioRxiv preprint doi: https://doi.org/10.1101/2023.04.04.535582; this version posted April 4, 2023. The copyright holder for this preprint (which was not certified by peer review) is the author/funder, who has granted bioRxiv a license to display the preprint in perpetuity. It is made available under aCC-BY-NC-ND 4.0 International license.

743 **Figure Legends**

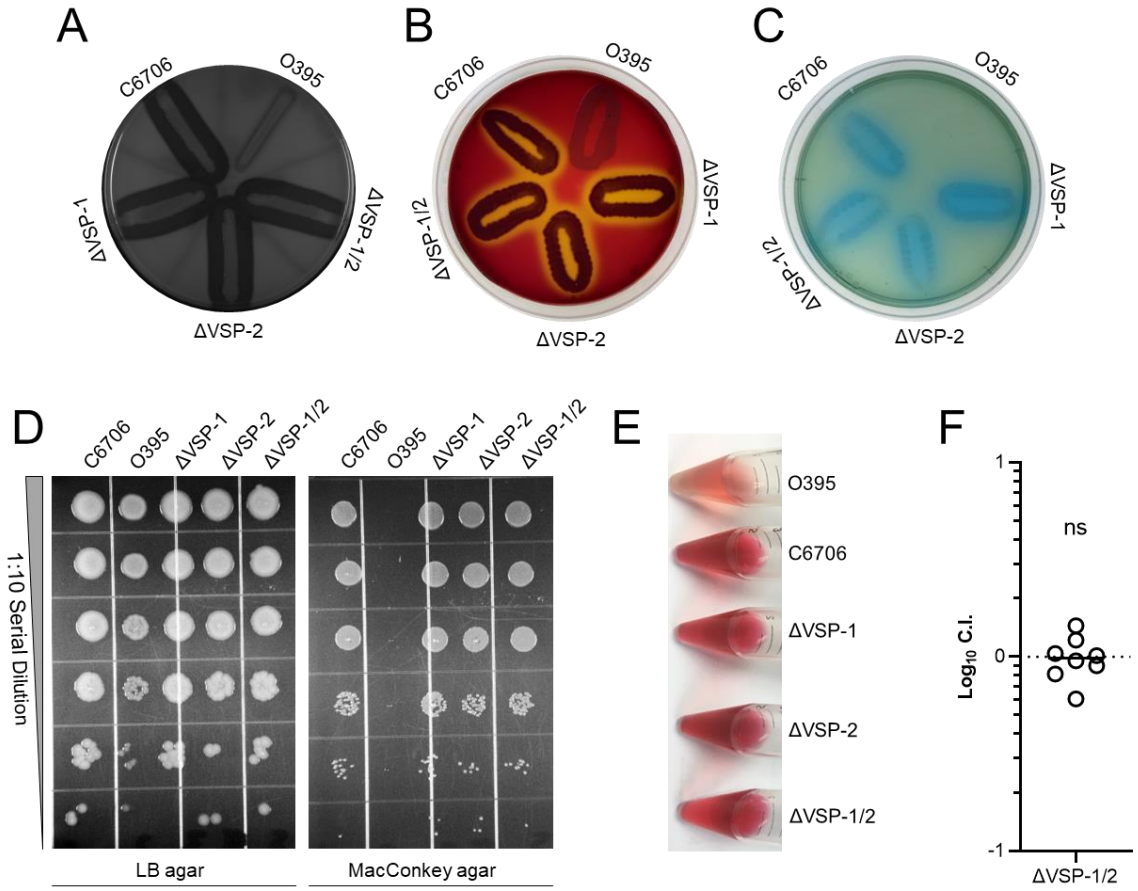

744

745 **Figure 1: The VSP islands do not contribute to common *V. cholerae* biotyping phenotypes**
746 **or virulence in a murine model of cholera.**

747 Differential biotyping phenotypes between classical O395, El Tor C6706, and C6706 VSP island
748 mutants (ΔVSP-1, ΔVSP-2, and ΔVSP-1/2) demonstrating strain specific (**A**) proteolysis of
749 casein on milk agar, (**B**) hemolytic activity on blood agar, (**C**) growth on citrate minimal medium
750 agar, (**D**) growth on matched LB and MacConkey agar plates, and (**E**) production of acetoin
751 detected by Voges-Proskauer Assay. All images are representative of three independent
752 experimental replicates. (**F**) In vivo competition between a 1:1 mixture of C6706 ΔVSP1/2 and
753 C6706 Δ*lacZ* in an infant mouse model of cholera. Intestinal colony forming units (CFU) were
754 enumerated using blue-white screening 20 hours after oral gavage. N = 8 mice and statistical
755 significance was determined using a one sample *t* test and a hypothetical mean Log_{10} C.I. = 0.
756 The hypothetical mean is represented by a dotted line. The calculated mean Log_{10} C.I. is
757 represented by a solid line. ns = not significant.
758

bioRxiv preprint doi: https://doi.org/10.1101/2023.04.04.535582; this version posted April 4, 2023. The copyright holder for this preprint (which was not certified by peer review) is the author/funder, who has granted bioRxiv a license to display the preprint in perpetuity. It is made available under aCC-BY-NC-ND 4.0 International license.

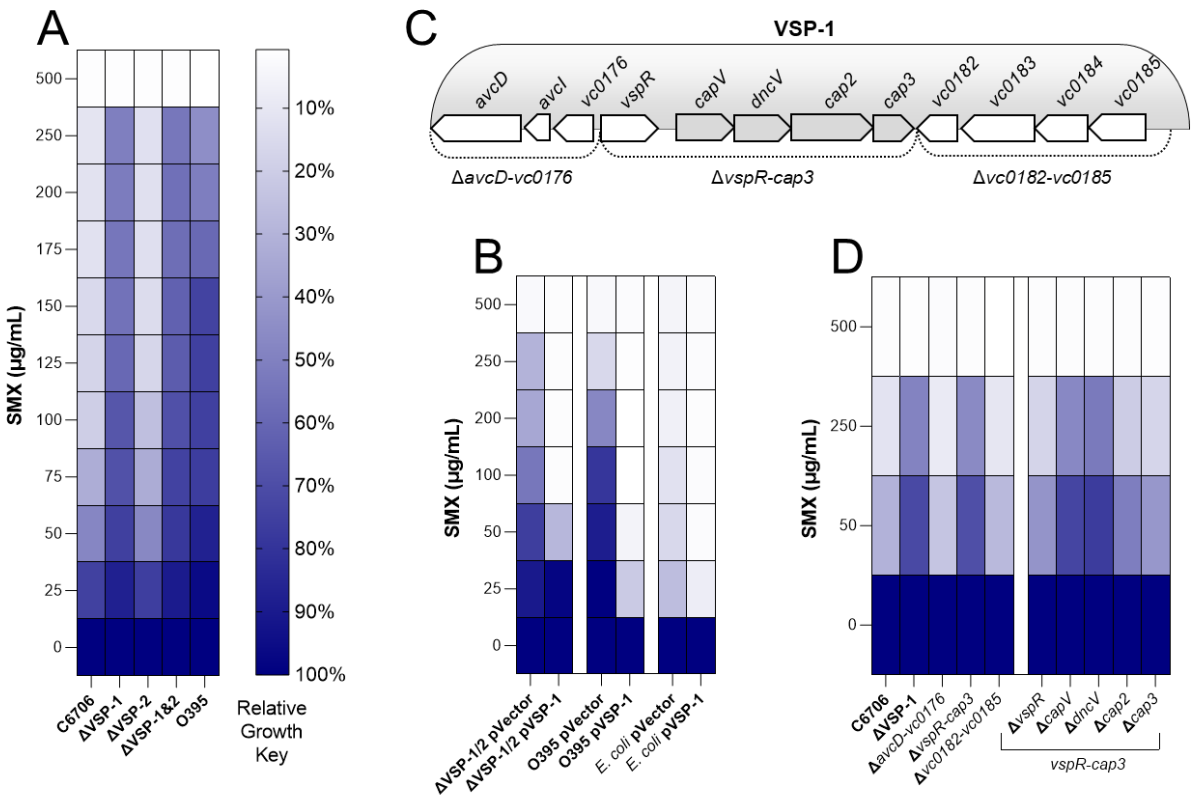

Figure 2: VSP-1 encoded CBASS is responsible for *V. cholerae* biotype specific SMX sensitivity.

24-hour planktonic antibiotic sensitivity assays were performed in a variety of SMX concentration gradients. Heatmaps (**A**), (**B**), and (**D**) represent relative growth for each strain calculated using culture optical densities and the equation (OD_{600} SMX treatment / OD_{600} untreated) and reported as a color-coded mean % of N = 3 biological replicates. The IC_{50} for all strains in (**A**) are presented in Supplementary Table 1. Scatter plots corresponding to (**A**) (**B**) and (**D**) are presented in (Figs. S2A-F). (**C**) Cartoon depiction of the VSP-1 genomic island. Dotted lines indicate partial VSP-1 truncations. Grey chevrons highlight the four gene VSP-1 CBASS operon.

bioRxiv preprint doi: https://doi.org/10.1101/2023.04.04.535582; this version posted April 4, 2023. The copyright holder for this preprint (which was not certified by peer review) is the author/funder, who has granted bioRxiv a license to display the preprint in perpetuity. It is made available under aCC-BY-NC-ND 4.0 International license.

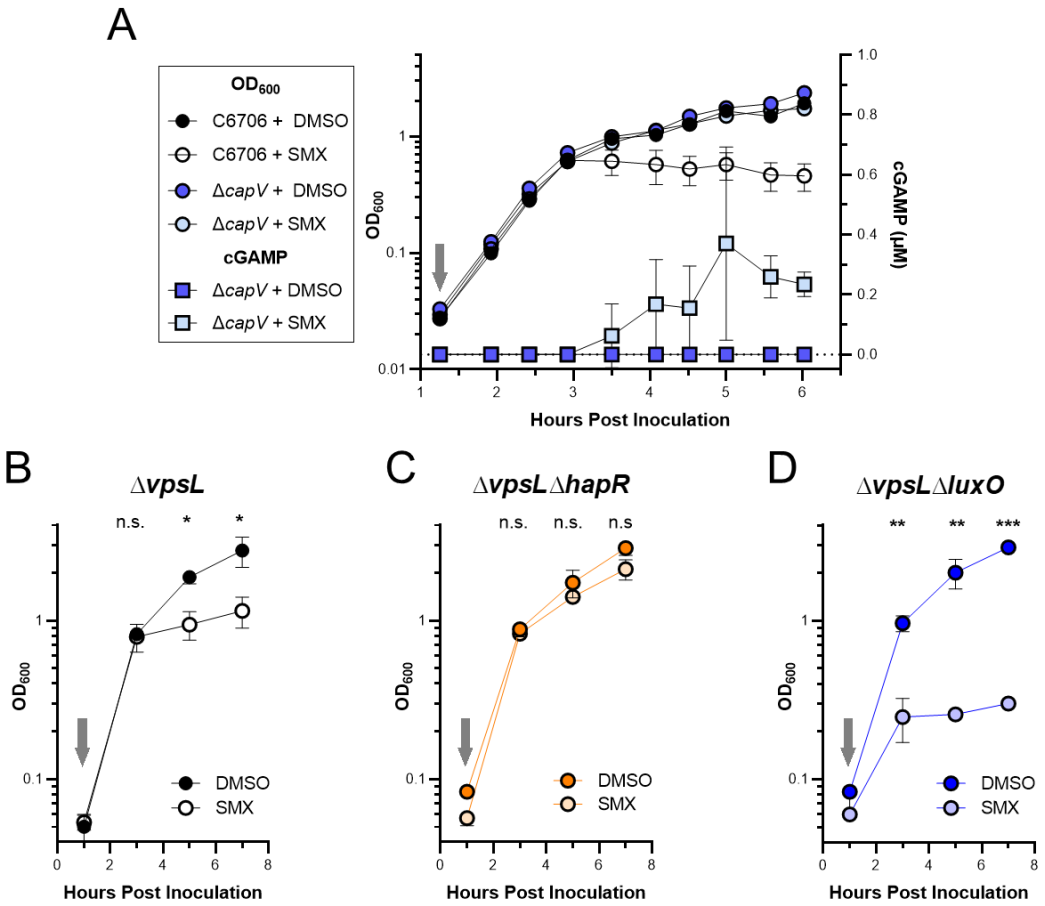

773

774 **Figure 3: Culture density-dependent sensitivity to SMX reveals quorum sensing regulation**
775 **of VSP-1 CBASS.**
776 (**A**) Growth curves (OD_{600}, left y-axis) of WT C6706 and Δ*capV* cultures treated without (+
777 DMSO) and with 100 μg/mL SMX (+ SMX). Intracellular cGAMP (μM, right y-axis) measured
778 by UPLC-MS/MS in the SMX treated and untreated Δ*capV* cultures. Growth curves of (**B**)
779 quorum fluent Δ*vpsL*, (**C**) LCD-locked Δ*vpsL*Δ*hapR*, and (**D**) HCD-locked Δ*vpsL*Δ*luxO* cultures
780 treated without (+ DMSO) and with 100 μg/mL SMX (+ SMX). Grey arrows indicate addition of
781 100 μg/mL SMX or DMSO. N = 3 biological replicates and error bars represent standard
782 deviation. Statistical significance calculated using an unpaired *t* test with the Holm-Šídák method
783 (*P < 0.05, **P < 0.005, ***P <0.0005), n.s. = not significant.
784

785

bioRxiv preprint doi: https://doi.org/10.1101/2023.04.04.535582; this version posted April 4, 2023. The copyright holder for this preprint (which was not certified by peer review) is the author/funder, who has granted bioRxiv a license to display the preprint in perpetuity. It is made available under aCC-BY-NC-ND 4.0 International license.

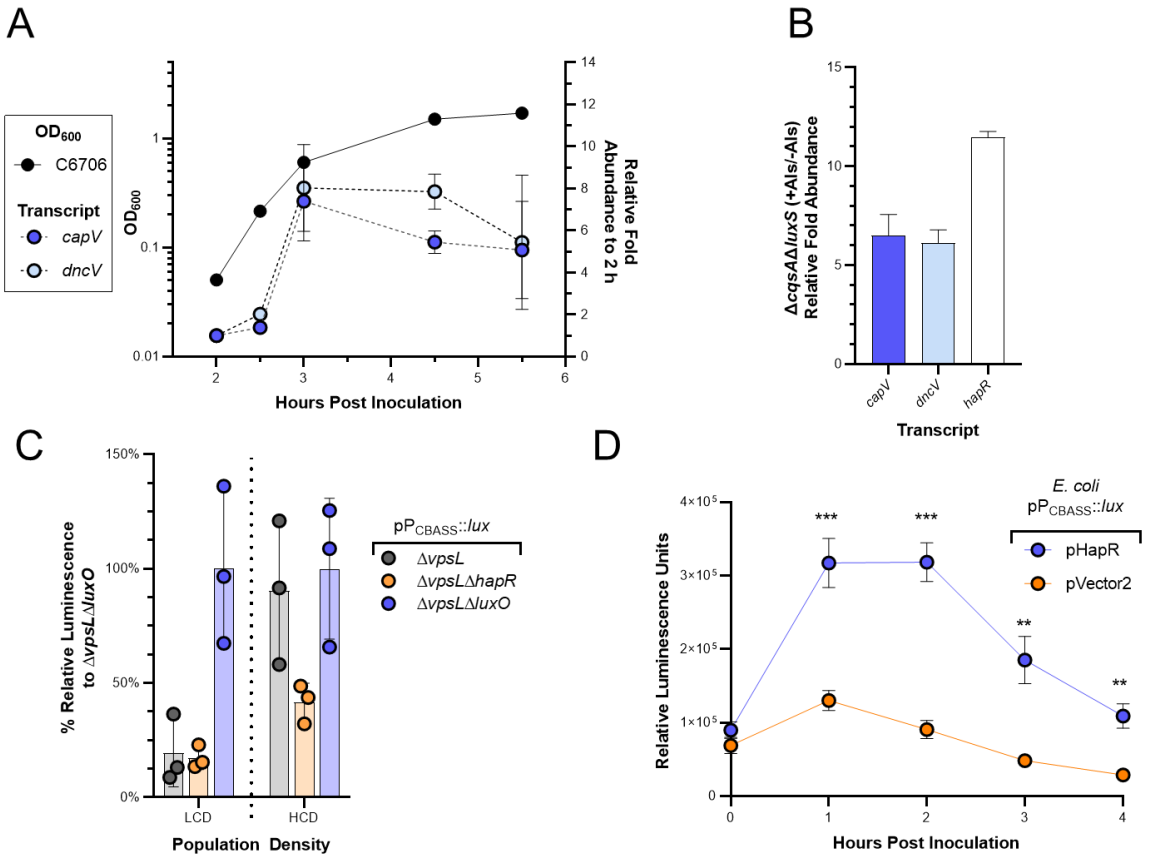

Figure 4: QS regulates expression of *V. cholerae* CBASS.
(**A**) Growth curve (OD_{600}, left y-axis, solid line) of *V. cholerae* C6706 and the corresponding fold-change in transcript abundance (right-axis) of *capV* and *dncV*, relative to the initial 2-hour time-point, measured using RT-qPCR. N = 2 biological replicates and error bars represent standard deviation. (**B**) Relative transcript abundance of *capV*, *dncV*, and *hapR* measured by qRT-PCR in Δ*csqA*Δ*luxS* grown in the presence (+) and absence (-) of exogenous autoinducers (AIs). N = 3 biological replicates and error bars represent standard error of the mean. (**C**) % relative luminescence units of the indicated strains normalized to the mean lum/OD_{600} of Δ*vpsL*Δ*luxO* maintaining the luminescent transcriptional reporter pP_{CBASS}::*lux.* Population densities are low-cell density (LCD) and high-cell density (HCD). N = 3 biological replicates and error bars represent standard deviation. (**D**) Relative luminescence (lum/OD_{600}) of *E. coli* maintaining the luminescent transcriptional reporter pP_{CBASS}::*lux* and the P_{tac} inducible *hapR* plasmid (pHapR) or a vector control (pVector2) grown in the presence of 6.25 µM IPTG. N = 3 biological replicates and error bars represent standard deviation. Statistical significance calculated using an unpaired *t* test with the Holm-Šídák method (**P < 0.005, ***P <0.0005), n.s. = not significant.

bioRxiv preprint doi: https://doi.org/10.1101/2023.04.04.535582; this version posted April 4, 2023. The copyright holder for this preprint (which was not certified by peer review) is the author/funder, who has granted bioRxiv a license to display the preprint in perpetuity. It is made available under aCC-BY-NC-ND 4.0 International license.

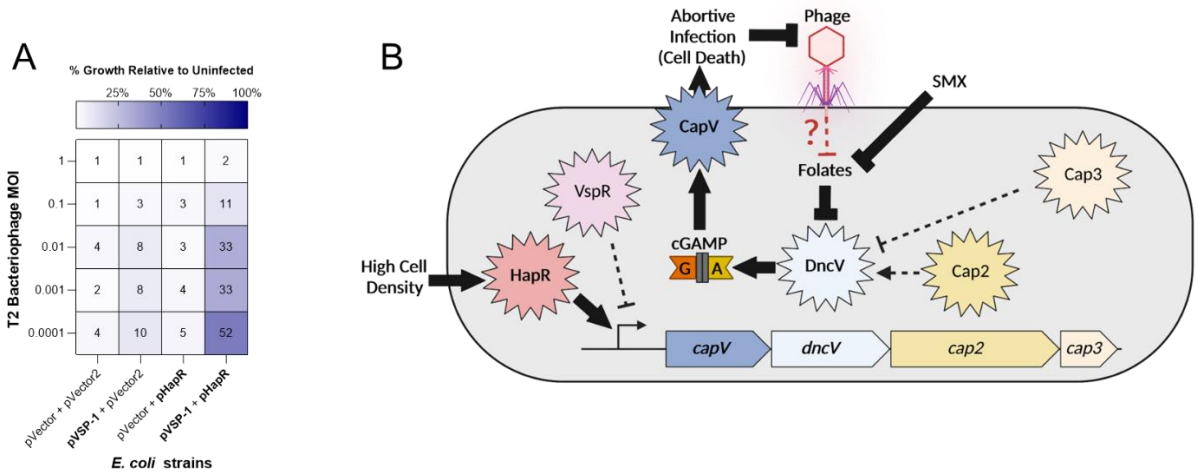

Figure 5: HapR enhances VSP-1 mediated phage defense in *E. coli*

(**A**) Growth of *E. coli* containing either pHapR induced with 10 μM IPTG and pVSP-1 with their associated vector controls after overnight growth with T2 phage is shown as a mean percent of the uninfected culture from N = 3 biological replicates. Mean % presented numerically and by heatmap for each condition. Scatter plot of data presented in (Fig. S4). (**B**) Model of folate (by SMX) and QS (by HapR) regulation of CBASS activity and expression. At HCD, HapR induces transcription of the CBASS operon. Inhibition of folate biosynthesis by SMX alleviates the folate-dependent non-competitive inhibition of DncV leading to synthesis of cGAMP and activation of the phospholipase CapV. CBASS activity ultimately culminates in abortive infection that thwarts phage predation by limiting phage replication. Solid arrows and brakes indicate regulatory mechanisms that influence CBASS activity addressed in this study. Black hatched arrows and brakes indicate mechanisms known to contribute to CBASS activity but were not found to significantly contribute to QS or folate mechanisms illuminated in this study. Red brake represents a hypothesized phage-dependent disturbance in folates which is sensed by DncV to initiate abortive infection by the *V. cholerae* CBASS. Created with BioRender.com.

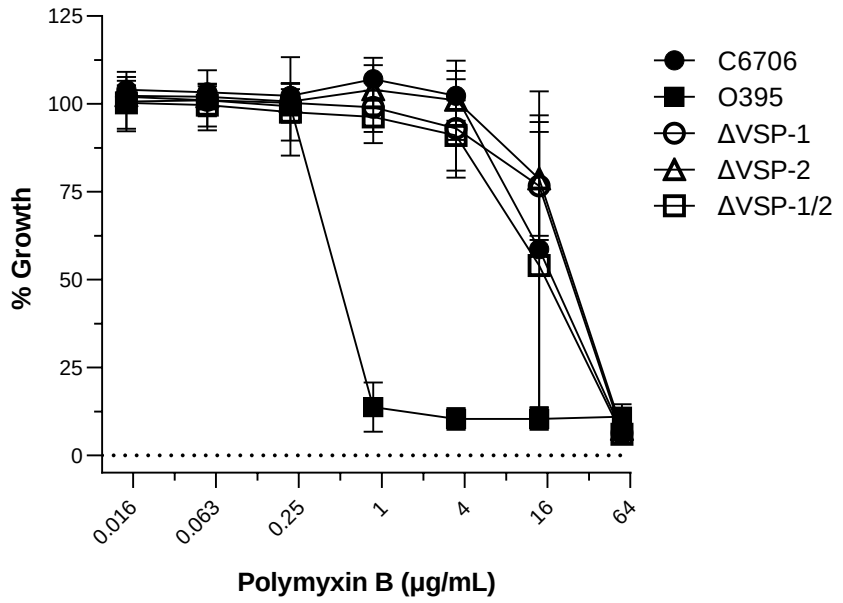

Figure S1: VSP-1 & -2 do not contribute to C6706 resistance to the antimicrobial peptide polymyxin B.

20-hour planktonic antibiotic sensitivity assay performed using a polymyxin B concentration gradient. % Growth reported as (OD_{600} polymyxin B treated / OD_{600} untreated) after 20 hours. Dotted line indicates 0% Growth. N = 3 biological replicates for all data points. Error bars represent standard deviation. IC_{50} for all strains are presented in Supplementary Table 1.

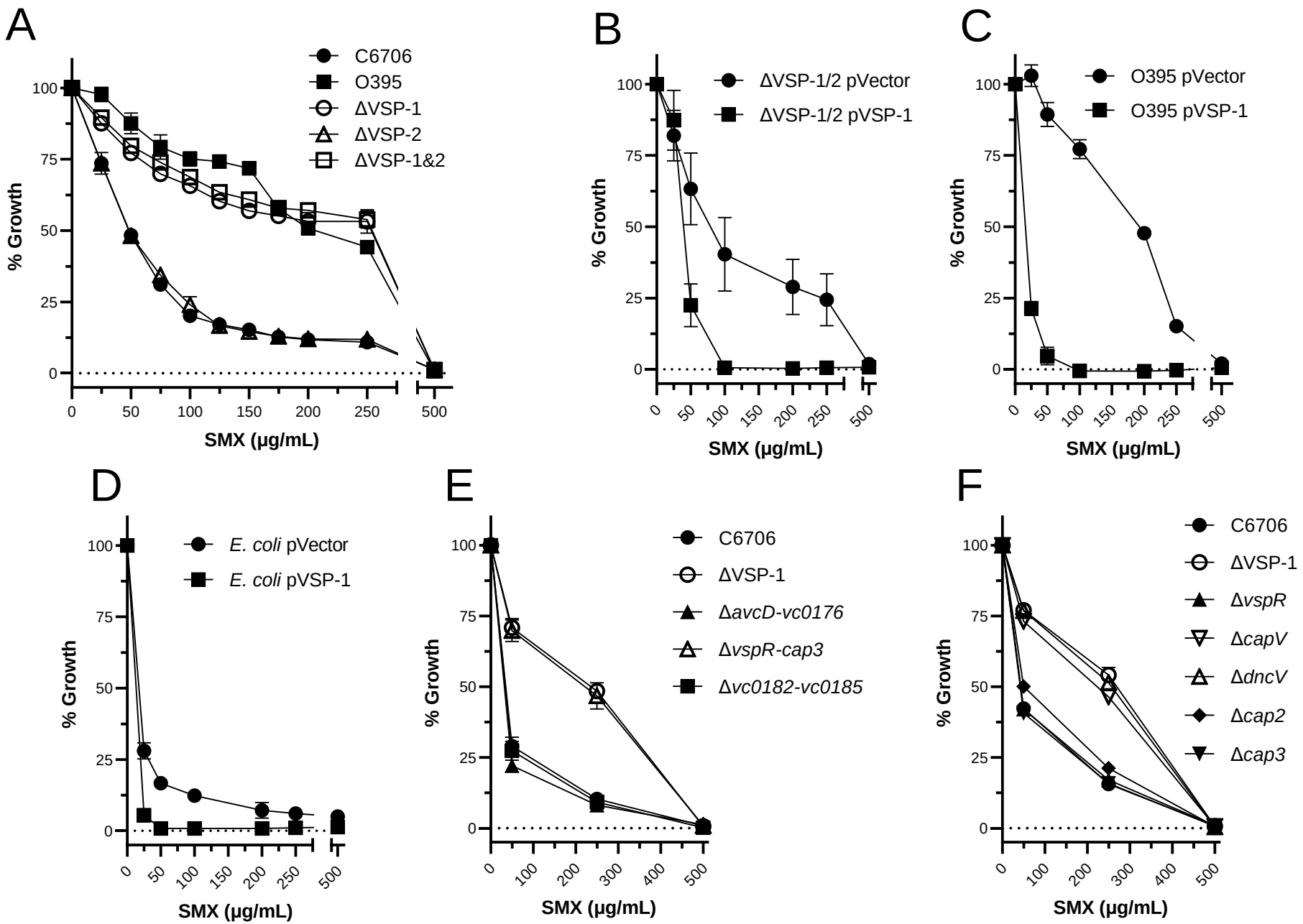
A
C6706
O395
ΔVSP-1
ΔVSP-2
ΔVSP-1&2
% Growth
SMX (μg/mL)
B
ΔVSP-1/2 pVector
ΔVSP-1/2 pVSP-1
% Growth
SMX (μg/mL)
C
O395 pVector
O395 pVSP-1
% Growth
SMX (μg/mL)
D
E. coli pVector
E. coli pVSP-1
% Growth
SMX (μg/mL)
E
C6706
ΔVSP-1
ΔavcD-vc0176
ΔvspR-cap3
Δvc0182-vc0185
% Growth
SMX (μg/mL)
F
C6706
ΔVSP-1
ΔvspR
ΔcapV
ΔdncV
Δcap2
Δcap3
% Growth
SMX (μg/mL)

Fig. S2

Figure S2: Scatter plots showing that VSP-1 encoded CBASS is responsible for *V. cholerae* biotype specific SMX sensitivity.

(**A-F**) 24-hour planktonic antibiotic sensitivity assays performed in a variety of SMX concentration gradients. Scatter plots represent are the same data presented in heatmap form in (Figs. 2A, 2B, & 2D). N = 3 biological replicates and error bars represent standard error of the mean. IC_{50} for all strains in (**A**) are presented in Supplementary Table 1.

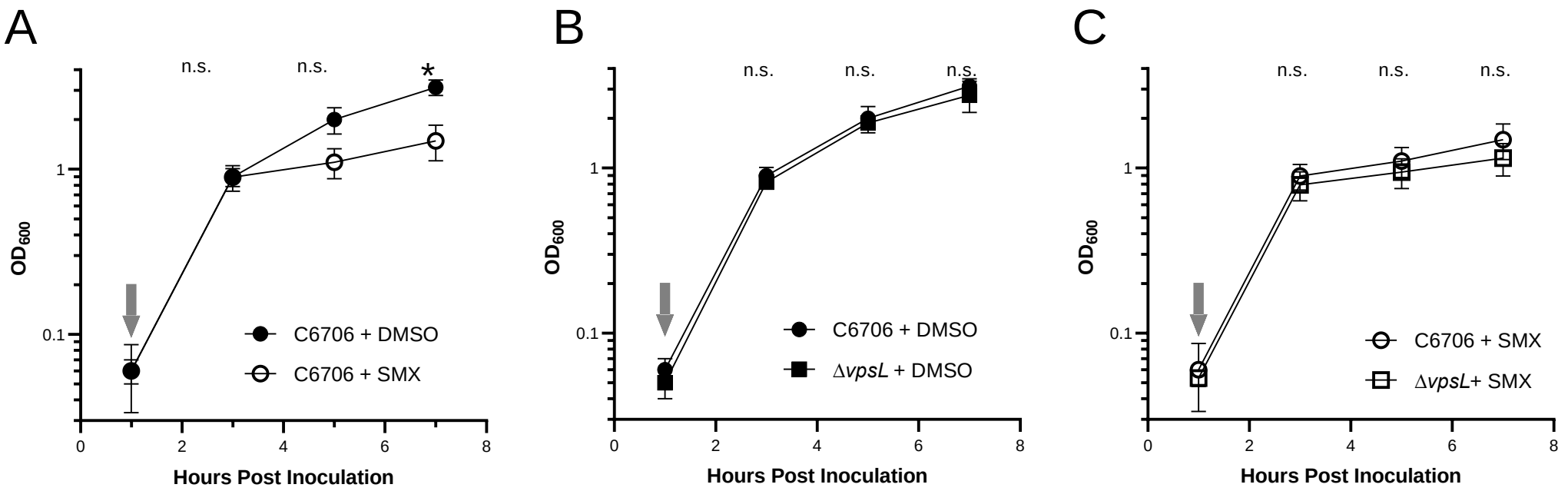

Figure S3: Lack of biofilm formation does not alter *V. cholerae* C6706 sensitivity to SMX.

Growth curves of (**A**) *V. cholerae* C6706 treated without (+ DMSO) and with 100 µg/mL SMX (+ SMX), and C6706 and Δ*vpsL* (**B**) untreated (+DMSO) and (**D**) treated (+SMX) with 100 µg/mL SMX. Grey arrows indicate addition of 100 µg/mL SMX or DMSO, approximately 1-hour after cultures were inoculated. N = 3 biological replicates and error bars represent standard deviation. For the purposes of statistical analysis, Δ*vpsL* data presented in (**B**) and (**C**) are also presented in (Fig. 3B). Statistical significance calculated using an unpaired *t* test with the Holm-Šídák method (*P < 0.05), n.s. = not significant.

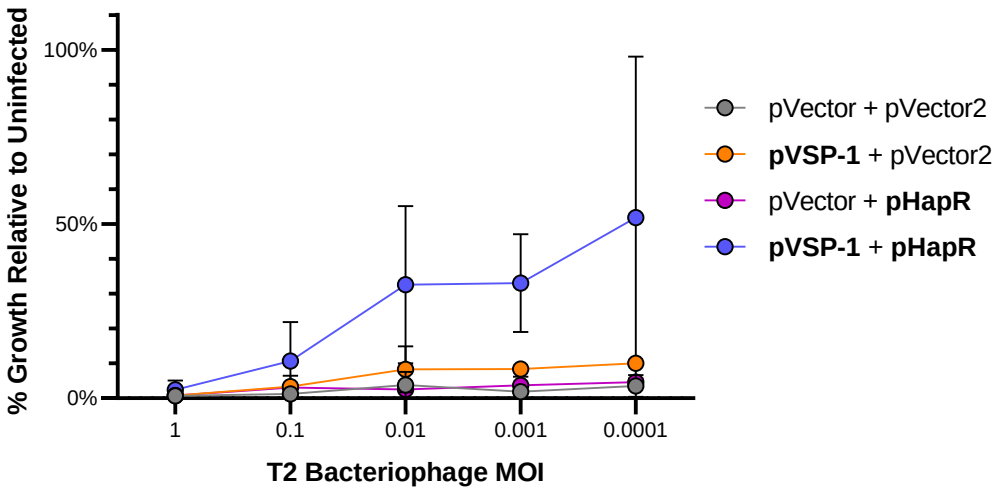

Figure S4: T2 phage infection graphs.

Growth of *E. coli* containing either pHapR induced with 10 μM IPTG and pVSP-1 with their associated vector controls after overnight growth with T2 phage. Data represent mean percent growth (OD_{600}) at the specified MOI calculated relative to control uninfected cultures. N = 3 biological replicates and error bars represent standard deviation. Data presented in heat map form in (Fig. 5A).

bioRxiv preprint doi: https://doi.org/10.1101/2023.04.04.535582; this version posted April 4, 2023. The copyright holder for this preprint (which was not certified by peer review) is the author/funder, who has granted bioRxiv a license to display the preprint in perpetuity. It is made available under aCC-BY-NC-ND 4.0 International license.

Supplementary Table 1: *V. cholerae* Antibiotic Sensitivity

Strain	Antibiotic	IC_{50} (μg/mL)	R^2
C6706	Polymyxin B	18.4	0.77
O395	Polymyxin B	0.6	0.85
ΔVSP-1	Polymyxin B	22.1	0.84
ΔVSP-2	Polymyxin B	24.8	0.81
ΔVSP-1/2	Polymyxin B	14.5	0.84
C6706	Sulfamethoxazole	36.5	0.95
O395	Sulfamethoxazole	230.7	0.82
ΔVSP-1	Sulfamethoxazole	184.7	0.85
ΔVSP-2	Sulfamethoxazole	38.0	0.95
ΔVSP-1/2	Sulfamethoxazole	207.2	0.85

IC_{50} and R^2 calculated using a non-linear regression analysis of
data presented in Fig. S1 (Polymyxin B) and Figs. 2A & S2A (Sulfamethoxazole)

Supplementary Table 2. Bacterial strains used in this study.

Strains	Name in this Study	Relevant Characteristics	Source or reference
Escherichia coli			
BL21(DE3)	*E. coli (for SMX treatment, Figs. 2B & S3D)*	*F- ompT hsdSB(rB -mB +) gal dcm (DE3)*	Lab Stock
BW29427	-	*RP4-2(TetSkan1360::FRT)*, *thrB1004*, *lacZ58*(M15), *ΔdapA1341::[erm pir+]*, *rpsL*(strR), *thi-*, *hsdS-*, *pro-*	Lab Stock
DH10b	*E.coli (for luminescence and phage challenge assays, Figs. 4C & 5A)*	*F-mcrA Δ(mrr-hsdRMS-mcrBC) Φ80lacZΔM15 ΔlacX74 recA1 endA1 araD139Δ(ara, leu)7697 galU galK λrpsL nupG*	ThermoFisher Scientific
Vibrio cholerae			
O395	O395	Wild type O1 classical; Sm^R	DiRita Lab Stock (23)
C6706str2	WT C6706	Wild type O1 El Tor; Sm^R -Quorum sensing proficient and does not contain the LuxO G333S quorum sensing variant found in some C6706 lineages (14)	Bassler Lab Lineage (8)
CR01	ΔVSP-1	C6706str2 ΔVSP-1	(8)
CR02	ΔVSP-2	C6706str2 ΔVSP-2	(8)
CR03	ΔVSP-1/2	C6706str2 ΔVSP-1/2	(8)
V. cholerae ΔlacZ (VC2338)	*ΔlacZ*	C6706str2 Δ*lacZ*	(59)
BYH255	Δ*acvD-vc0176*	C6706str2 Δ*acvD-vc0176*	(8)
BYH256	Δ*vspR-cap3*	C6706str2 Δ*vspR-cap3*	(8)
BYH257	Δ*vc0182-vc0185*	C6706str2 Δ*vc0182-vc0185*	(8)

bioRxiv preprint doi: https://doi.org/10.1101/2023.04.04.535582; this version posted April 4, 2023. The copyright holder for this preprint (which was not certified by peer review) is the author/funder, who has granted bioRxiv a license to display the preprint in perpetuity. It is made available under aCC-BY-NC-ND 4.0 International license.

GS07	Δ*vspR*	C6706str2 Δ*vspR* (not a deletion but a variant with nonsense mutations in codons 1, 2, and 6)	This study
WLN5105	Δ*capV*	C6706str2 Δ*capV*	(10)
GS01	Δ*dncV*	C6706str2 Δ*dncV*	(10)
WLN5380	Δ*cap2*	C6706str2 Δ*cap2*	(10)
WLN5381	Δ*cap3*	C6706str2 Δ*cap3*	(10)
CW2034	Δ*vpsL*	C6706str2 Δ*vpsL* biofilm-null	(35)
CW2036	Δ*vpsL*Δ*hapR*	C6706str2 Δ*vpsL* biofilm-null LCD-locked	(35)
CW2037	Δ*vpsL*Δ*luxO*	C6706str2 Δ*vpsL* biofilm-null HCD-locked	(35)
BH1842	*ΔcsqAΔluxS*	C6706str2 *ΔcsqAΔluxS*, LCD-locked with HCD induction by exogenous AIs	(37)
Phage			
T2	T2	Wild type	ATCC

Supplementary Table 3: Plasmids used in this study

Plasmids	Name in this Study	Relevant characteristics	Source or Reference
pLAFR	pVector	pLAFR cosmid; Tet^r	(64)
pCCD13	pVSP-1	pLAFR containing VSP-1; Tet^r	(10)
pBBR-lux	-		(57)
pKAD1	pP_{CBASS}::*lux*	pBBRlux containing 913bp 5' of *capV* locus (*i.e.,* CBASS promoter) to regulate luciferase expression	This study
pGBS54	-	pKAS32; Amp^r containing homologous region for introducing *vspR* nonsense mutations (creating strain GS07)	This study
pSLS13	pHapR	*hapR* allele cloned into pEVS143 under P_{tac}	(63)
pEVS141	pVector2	Promoterless pEVS143 vector control	(62)

Supplementary Table 4: Oligonucleotides used in this study

Name	Primer use	Sequence	Reference
Vector Construction Primers			
DS fwd VC0177 start stop	Construction of pGBS54	TAGTGACGTTCTATGTAGATCAGTGCAGAG	This study
DS rev VC0177 start stop	Construction of pGBS54	CTATAGTTCTAGAGGTACCTATGTCCTTTCAAAAAGCAAG	This study
US fwd VC0177 start stop	Construction of pGBS54	ATTCCCGGGAGAGCTGTGGTATGAAAGATGAGTGAAATAC	This study
US rev VC0177 start stop	Construction of pGBS54	CTACATAGAACGTCACTAGTATTTCTAATACCAC	This study
Lux_CBASSpr_FW	PCR P_{CBASS} region Rev (913 nt 5' *capV*) into pBBR-lux	CACCGCGGTGGCGGCCGCTCTAGAAAACGATATATAACCAAAGATCAAG	This study
Lux_CBASSpr_RV	PCR P_{CBASS} region Rev (913 nt 5' *capV* pBBR-lux	GGATTGAAAACGGAGGTTACCTCTAGTTGCGGCCGCAAAATGGAT	This study
RT-qPCR Primers			
CMW2926	*gyrA* F, housekeeping gene (Fig. 4A)	TGGCCAGCCAGAGATCAAG	(8)

bioRxiv preprint doi: https://doi.org/10.1101/2023.04.04.535582; this version posted April 4, 2023. The copyright holder for this preprint (which was not certified by peer review) is the author/funder, who has granted bioRxiv a license to display the preprint in perpetuity. It is made available under aCC-BY-NC-ND 4.0 International license.

CMW2927	*gyrA* R, housekeeping gene (Fig. 4A)	ACCCGCAGCGGTACGA	(8)
*capV*a F qPCR	*capV* F (Fig. 4A)	GTGCGCTTGGATAACAACATAC	This study
*capV*a R qPCR	*capV* R (Fig. 4A)	TACCGCGGCTAGCTAAATTAC	This study
*dncV*b F qPCR	*dncV* F (Fig. 4A)	ACAGACGAGGAGAAGAACAATC	This study
*dncV*b R qPCR	*dncV* R (Fig. 4A)	AGCCTTGGCAATACCCTTAG	This study
WNTP0011	*recA* F, housekeeping gene (Fig. 4B)	AATTTGTGATGCACTGGCTCGCTC	This study
WNTP0012	*recA* R, housekeeping gene (Fig. 4B)	CGTCAGTTTACGCATTGCTTGCGA	This study
WNTP1492	*capV* F (Fig. 4B)	CTTTGCAGATGGGGGATTGGTTGC	This study
WNTP1493	*capV* R (Fig. 4B)	CCTTTGCTTCAGGAAAGTCTGTTGCC	This study
WNTP1494	*dncV* F (Fig. 4B)	GCACCTTTCTGACAGCGAACAACG	This study
WNTP1495	*dncV* R (Fig. 4B)	GTCCAAAAGCGAGGTGTCAATCCC	This study
WNTP0015	*hapR* F (Fig. 4B)	CGTGACGAAGTTTGGCCACTGTTT	This study
WNTP0016	*hapR* R (Fig. 4B)	TGTTTCTCACACAATTCGCCACGC	This study